A highly sensitive cell-based luciferase assay for high-throughput automated screening of SARS-CoV-2 nsp5/3CLpro inhibitors

K.Y. Chen, T. Krischuns, L. Ortega Varga, E. Harigua-Souiai, S. Paisant, A. Zettor, J. Chiaravalli, A. Delpal, D. Courtney, A. O'Brien, et al.

▶ To cite this version:

A highly sensitive cell-based luciferase assay for high-throughput automated screening of SARS-CoV-2 nsp5/3CLpro inhibitors

K.Y. Chen [a,2], T. Krischuns [a,2], L. Ortega Varga [b,2], E. Harigua-Souiai [c], S. Paisant [a], A. Zettor [d], J. Chiaravalli [d], A. Delpal [g], D. Courtney [a,1], A. O'Brien [e], S.C. Baker [e], E. Decroly [g], C. Isel [a], F. Agou [d], Y. Jacob [f], A. Blondel [b], N. Naffakh [a,*]

[a] Institut Pasteur, Université Paris Cité, CNRS UMR3569, Unité Biologie des ARN et Virus Influenza, F-75015 Paris, France
[b] Institut Pasteur, Université Paris Cité, CNRS UMR3528, Unité de Bioinformatique Structurale, F-75015 Paris, France
[c] Laboratory of Molecular Epidemiology and Experimental Pathology – LR16IPT04, Institut Pasteur de Tunis, Université de Tunis El Manar, Tunis, Tunisia
[d] Institut Pasteur, Université Paris Cité, CNRS UMR3523, Plateforme de Criblage Chémogénomique et Biologique, F-75015 Paris, France
[e] Department of Microbiology and Immunology, Loyola University Chicago, Stritch School of Medicine, Maywood, IL, USA
[f] Institut Pasteur, Université Paris Cité, CNRS UMR3569, Unité Génétique Moléculaire des Virus à ARN, F-75015 Paris, France
[g] Architecture et Fonction des Macromolécules Biologiques, Aix-Marseille Université, CNRS UMR7257, F-13009 Marseille, France

ARTICLE INFO

ABSTRACT

Effective drugs against SARS-CoV-2 are urgently needed to treat severe cases of infection and for prophylactic use. The main viral protease (nsp5 or 3CLpro) represents an attractive and possibly broad-spectrum target for drug development as it is essential to the virus life cycle and highly conserved among betacoronaviruses. Sensitive and efficient high-throughput screening methods are key for drug discovery. Here we report the development of a gain-of-signal, highly sensitive cell-based luciferase assay to monitor SARS-CoV-2 nsp5 activity and show that it is suitable for the screening of compounds in a 384-well format. A benefit of miniaturisation and automation is that screening can be performed in parallel on a wild-type and a catalytically inactive nsp5, which improves the selectivity of the assay. We performed molecular docking-based screening on a set of 14,468 compounds from an in-house chemical database, selected 359 candidate nsp5 inhibitors and tested them experimentally. We identified two molecules which show anti-nsp5 activity, both in our cell-based assay and *in vitro* on purified nsp5 protein, and inhibit SARS-CoV-2 replication in A549-ACE2 cells with EC_{50} values in the 4–8 μM range. The here described high-throughput-compatible assay will allow the screening of large-scale compound libraries for SARS-CoV-2 nsp5 inhibitors. Moreover, we provide evidence that this assay can be adapted to other coronaviruses and viruses which rely on a viral protease.

1. Introduction

In January 2020, a novel human coronavirus named severe acute respiratory syndrome coronavirus 2 (SARS-CoV-2) was identified as the causative agent of the COVID-19 disease. SARS-CoV-2 has spread globally, causing a pandemic that is still on-going and has to date infected over 450 million people and caused over 6 million deaths worldwide (John Hopkins University & Medicine, 2022). Vaccines started to be deployed early 2021 and more than 10 billion doses have been administered to date (John Hopkins University & Medicine, 2022). However,

until complete vaccine coverage will be reached and with the emergence of variants of concern, there is a critical need for prophylactic and therapeutic antiviral drugs. Despite huge efforts, only few treatments have been approved or authorized under emergency use authorization until december 2021 (US Food and Drug Administration, 2022), among which the glucocorticoid dexamethasone (Group et al., 2021) and the IL6 receptor blocker tocilizumab (Rosas et al., 2021), which show a benefit in severe COVID-19 cases. Other authorized treatments during that period include the REGEN-COV antibody cocktail (O'Brien et al., 2021a), whose high cost precludes large-scale administration and whose

efficacy was reduced against the Omicron variant (Planas et al., 2021), and the ribonucleotide analog remdesivir whose efficacy is limited (Beigel et al., 2020). In December 2021, two antivirals were authorized for clinical use: molnupiravir and PF-07321332, that target the RNA polymerase and the main protease of SARS-CoV-2, respectively (Fischer et al., 2022; Hammond et al., 2022; Owen et al., 2021; Zhao et al., 2021).

SARS-CoV-2 is an enveloped virus with a positive-, single-stranded RNA genome. It belongs to the *Coronaviridae* family, which includes other zoonotic coronaviruses (SARS-CoV-1 and the Middle-East Respiratory Syndrome Coronavirus or MERS-CoV) as well as human seasonal coronaviruses that cause common colds. The large open reading frame ORF1ab at the 5′ end of the SARS-CoV-2 genome is translated into two viral polyproteins that are cleaved by two viral proteases into at least 16 non-structural proteins (nsps) (V'Kovski et al., 2021). The main protease is a chymotrypsin-like cysteine-dependent protease called nsp5 (or 3CLpro or Mpro), and the second protease is a papain-like protease domain within nsp3 called PLpro (for a review see Ullrich and Nitsche, 2020). Both proteases represent attractive targets for drug development as they are essential to the progression of the viral life cycle, and their active sites are highly conserved among betacoronaviruses. Nsp5 is a dimer composed of two identical monomers of 306 residues, while the PLpro region of nsp3 is 317 residues long and composed of 4 sub-domains, including an ubiquitin-like domain. Nsp5 is considered to be a particularly attractive target because it cleaves the viral replicase polyprotein 1 ab at 11 major cleavage sites and is required to produce the RNA-dependent RNA polymerase complex (nsp12-nsp7-nsp8), and because its cleavage specificity is distinct from human proteases. To date, there are more than 250 structures available in the Protein Data Bank (PDB, Berman et al., 2000) database for the SARS-CoV-2 nsp5, including complexes with small molecules, which facilitates structure-based design of new antivirals (Dai et al., 2020; Gunther et al., 2021; Jin et al., 2020; Khan et al., 2020; Wang et al., 2020; Zhang et al., 2020). Early on, the lopinavir/ritonavir protease inhibitor cocktail that prevents HIV replication was proposed as an antiviral agent against SARS-CoV-2, however clinical trials did not demonstrate benefits in patients with severe COVID-19 (Cao et al., 2020). Boceprivir, a protease inhibitor used to treat patients with Hepatitis C virus (genotype 1) chronic infection, showed only a moderate activity against SARS-CoV-2 nsp5 (Hu et al., 2021; Ma et al., 2020, 2021) and was not tested in COVID-19 clinical trials. The covalent peptidomimetics PF-00835231 initially developed by the Pfizer company against SARS-CoV-1 and MERS-CoV and its prodrug PF-07304814 turned out to be active against SARS-CoV-2 (Boras et al., 2021). Pfizer announced in November 2021 that its novel oral antiviral Paxlovid, a combination of PF-07321332 and ritonavir, reduced the risk of hospitalization or death by nearly 90% compared to placebo in interim analysis of a Phase 2/3 trial in high-risk adults with COVID-19 (Hammond et al., 2022; Owen et al., 2021). Only a few other candidate protease inhibitors, notably Masitinib (Drayman et al., 2021) and S-217622 (Shionogi, 2022) are currently being evaluated in clinical trials.

Paxlovid has been authorized for use by the FDA in December 2021 and by the EMA in January 2022, which represents a major advance for pandemic management. Although the structure of the active site of nsp5 is highly conserved among coronaviruses, and its sequence shows very few variations among the >1.9 millions SARS-CoV-2 full-genome available to date (Gao et al., 2021), the emergence of viruses with drug-resistant mutations cannot be excluded. The identification of other anti-SARS-CoV-2 drugs therefore remains a high priority. Sensitive and efficient high-throughput screening methods are key for the discovery of additional novel protease inhibitors. *In vitro* biochemical assays, which assess the protease activity of purified SARS-CoV-2 nsp5 are available (Fu et al., 2020; Hung et al., 2020; Jin et al., 2020; Rathnayake et al., 2020; Zhang et al., 2020; Zhu et al., 2020). However, *in vitro* assays need to be complemented with cell-based assays as they do not take into account compound membrane permeability, toxicity and bioavailability in cells. Cell-based reporter assays that can be performed in a Biosafety

Level 1 (BSL1) setting have been developed (Froggatt et al., 2020; O'Brien et al., 2021b; Rawson et al., 2021; Resnick et al., 2021; Rothan and Teoh, 2021) but their suitability for high-throughput screening has not been demonstrated. Here we report the development of a rapid and highly sensitive cell-based luciferase assay to monitor SARS-CoV-2 nsp5 activity. We provide evidence that the reporter assay is suitable for high-throughput automated screening of large libraries of compounds and report the identification of two lead compounds that inhibit protease activity in our cell-based assay and *in vitro* on purified nsp5 protein, and inhibit SARS-CoV-2 replication in cell culture.

2. Material and methods

Antibodies and Virtual screening for anti-nsp5 compounds are described in the Supplementary Methods.

2.1. Cells and virus

HEK-293T cells (designated as HEK-293T/17 from ATCC, # CRL-11268) and A549 cells stably expressing the human ACE2 receptor (A549-ACE2, kindly provided by O. Schwartz, Institut Pasteur) were grown in complete Dulbecco's modified Eagle's medium (Gibco) supplemented with 10% fetal bovine serum (FBS). Blasticidin was added to the A549-ACE2 medium at a concentration of 10 μg/mL to maintain the expression of ACE2. The BetaCoV/France/IDF0372/2020 virus was kindly provided by S. van der Werf (Institut Pasteur).

2.2. Plasmids

The pcDNA3.1 expression vectors for a SARS-CoV-2 polyprotein corresponding to the non-structural proteins 4, 5 and the N-terminal part of nsp6 (designated CoV-2-nsp4-5-6 WT), and its catalytically inactive counterpart in which cysteine 145 (with numbering starting at the first residue of nsp5) was changed to alanine (designated CoV-2-nsp4-5-6 C145A) are described in (O'Brien et al., 2021b). The mutated cleavage site between nsp5 and 6 was changed to the wild-type sequence by site-directed mutagenesis. These plasmids were used as templates to amplify the sequence encoding nsp5 (WT or C145A), and the resulting amplicons were subcloned into the pcDNA3.1 plasmid. The pLEX expression vectors for SARS-CoV-2, IBV and hCoV-229E nsp5 are described in (Froggatt et al., 2020) and were kindly provided by N. Heaton (Duke University). The pGEX-6P-1 plasmid used to produce the recombinant nsp5 was kindly provided by R. Hilgenfeld (University of Luebeck) (Zhang et al., 2020). The Hepatitis C Virus (HCV) NS3/4A expression vector was generated by subcloning a synthetic gene which was codon optimized for expression in human cells (Genscript) into the pCI plasmid. Site-directed mutagenesis was performed to generate a catalytically inactive mutant in which S139 (with numbering starting at the first residue of NS3) was changed to alanine (designated HCV-NS3/4A S139A). To generate the Reverse-Nanoluciferase reporter plasmid Rev-Nluc-CoV, a synthetic codon-optimized nucleotide sequence encoding a permuted Nanoluciferase with the NGSVRLQSSLK linker between the N- and the C-terminal domains was cloned into the pLV-CMV-eGFP lentiviral vector (Duke vector core, Duke University) in place of the eGFP insert. The other Rev-Nluc reporter plasmids were produced in two steps. First, a synthetic codon-optimized nucleotide sequence encoding a permuted Nanoluciferase with two BsmBI sites between the N- and the C-terminal domain was cloned into pLV-CMV-eGFP. Second, double-stranded oligonucleotides encoding alternative nsp5, Tobacco Etch Virus (TEV) or HCV-NS3/4A protease cleavage sites were cloned in frame using the BsmBI sites. All constructs were verified by sequencing. Primers used for cloning and mutagenesis are available upon request.

2.3. Viral protease activity assays

HEK-293T cells were seeded in 96-well white opaque plates (Greiner Bio-One, 3×10^4 cells per well) one day before being transfected with 5 ng of the Rev-Nluc-CoV reporter plasmid and 95 ng of the pcDNA3.1-nsp4-5-6 WT, pcDNA-3.1-nsp4-5-6 C145A, pLEX-nsp5 or an empty control pCI plasmid, using polyethyleneimine (PEI-max, #24765–1 Polysciences Inc). To measure NS3/4A activity, 5 ng of the Rev-Nluc-HCV reporter plasmid was co-transfected with 145 ng of the pCI-NS3/4A WT or pCI-NS3/4A S139A, using the same protocol. Nanoluciferase activity was measured at 24 or 48 h post-transfection (hpt) using the Nano-Glo® Luciferase Assay System (#1120, Promega) and a Berthold Centro XS3 luminometer (integration time 1s/well using the Mikro-Win® software). When indicated, cells were treated at 8 hpt with increasing concentrations of the inhibitors GC376 (Sigma-Aldrich), Calpain Inhibitor XII (Cayman Chemicals), Mpro 13b (Bio-Techne), Boceprevir (Sigma-Aldrich) and PF-07321332 (MedChem Express) with a constant DMSO concentration of 0.1%, for ~14 h. Nanoluciferase activity was measured at 24 hpt.

In the 384-well plate setting, $\sim10^7$ HEK-293T cells were transfected in 50 cm^2 dishes with 1 µg of the Rev-Nluc-CoV plasmid and 15 µg of the nsp4-5-6 WT or nsp4-5-6 C145A expression plasmids. Increasing amounts of the tested compounds, corresponding to final concentrations of 0.1–50 µM with a constant DMSO concentration of 0.5% were distributed in 384-well white opaque plates using an Echo 555 Liquid Handler (Labcyte). Transfected HEK-293T cells were trypsinized at 6 hpt and distributed in the 384-well plates (2×10^4 cells per well in 50 µL). The luciferase activity was measured at 24 hpt as described above. A Tecan-Fluent robotic workstation was used to dispense cells and luciferase substrate. Each 384-well plate included 14 negative control wells (mean DMSO-treated signal = DMSO) and 14 positive-control wells (mean GC376 at 50 µM signal = GC). The IC$_{50}$ values were determined using the CDD Vault software (Collaborative Drug Discovery) and normalization of compound-treated signals (C) as follows: (C - DMSO)/(GC – DMSO) x 100 in nsp4-5-6 WT expressing cells, and (C/DMSO) x 100 in nsp4-5-6 C145A expressing cells. The z' factor calculated for each plate using the CDD software (z' = 1- [3 x $(\sigma_p + \sigma_n)/|\mu_p - \mu_n|$], where σ_p and σ_n are the standard deviation of the positive and negative controls, respectively, and μ_p and μ_n are the mean of the positive and the negative controls, respectively) was around 0.8.

Additional information about tested compounds (MolPort Compound number, supplier, purity) is provided in the Supplemental Methods section.

2.4. Nsp5 protein purification and in vitro activity assay

The nsp5 protein was produced in E. coli as previously described (Zhang et al., 2020). Briefly, the pGEX-6P-1 plasmid was transformed in E coli BL21 DE3 gold, and the nsp5 protein was produced overnight at 17 °C upon IPTG induction (250 µM). Bacterial pellets were resuspended in lysis buffer (50 mM Tris pH 8, 300 mM NaCl, 5 mM MgSO$_4$, 10% Glycerol, 0.1%Triton X-100, supplemented with 0.25 mg/mL Lysozyme, 1 mM PMSF, and 10 µg/mL DNAse I). After 3 cycles of sonication and clarification, the 6xHis-tagged protein was purified by NTA affinity on cobalt beads, and the nsp5 protein was eluted in lysis buffer supplemented with 250 mM imidazole. The nsp5 protein was then concentrated on Vivaspin 20 centrifugal concentrators 10 kDa MWCO (GE Healthcare #VS2001), dialysed against the elution buffer in the absence of imidazole, and stored at −80 °C upon addition of 50% glycerol.

The fluorescence resonance energy transfer (FRET)-based *in vitro* activity assays were performed in black 384-well HiBase non-binding plates (Greiner Bio One #784900). Briefly, serial dilution of the inhibitors were incubated with purified nsp5 protein (80 nM) and 5 µM of a florescent synthetic peptide (Dabcyl-KTSAVLQ↓SGFRKM-Edans-NH2, purchased from Genscript) in HEPES buffer (20 mM, pH 6.5) containing 120 mM NaCl, 0.4 mM EDTA, 4 mM DTT and 10% glycerol. The DMSO

final concentration was adjusted at 0.5%. Cleavage of the synthetic peptide by nsp5 separates the Edans/Dabcyl fluorophore-quencher pair. The time courses of the enzymatic reaction were followed during 40 mn by monitoring the increase of fluorescence emission at 493 nM (excitation 335 nM) using a Tecan Saphir 2 fluorimeter during 40 mn. The enzymatic activities were estimated by taking the slope of the linear part of the reaction curve, and were normalized with respect to the activity measured in the absence of inhibitor. The IC$_{50}$ values were determined by plotting the % of activity as a function of the inhibitor concentration and by fitting the curves with Prism (GraphPad) using the following equation: Y = 100/(1+((X/IC$_{50}$)^Hill slope).

2.5. Antiviral activity and cell viability assays

A549-ACE2 cells seeded in 384-well plates (1.5×10^3 cells per well) were incubated with the compound of interest at the indicated concentration in DMEM-2% FBS for 2 h prior to infection. The media was replaced with the SARS-CoV-2 inoculum (MOI = 0.1 Particle Forming Unit per cell) and incubated for 1 h at 37 °C. The inoculum was removed and replaced with drug-containing media. At 72 h post infection (hpi), the cell culture supernatant was collected, heat inactivated at 80 °C for 20 min, and used for RT-qPCR analysis. The Luna Universal One-Step RT-qPCR Kit (New England Biolabs) was used, with SARS-CoV-2 specific primers targeting the N gene region (5′-TAATCAGA-CAAGGAACTGATTA-3′ and 5′-CGAAGGTGTGACTTCCATG-3′) and with the following cycling conditions: 55 °C for 10 min, 95 °C for 1 min, for 1 cycle, followed by 95 °C for 10 s, 60 °C for 1 min, for 40 cycles in an Applied Biosystems QuantStudio 6 thermocycler. The percentage of viral growth inhibition was calculated as the ratio of the sample mean Ct to the positive control (remdesivir 1 µM) mean Ct, after subtracting the negative control (DMSO 0.5%) mean Ct. Cell viability assays were performed in drug-treated cells using the CellTiter-Glo assay according to the manufacturer's instructions (Promega) and a Berthold Centro XS LB960 luminometer. The percentage of cytotoxicity was calculated relative to untreated cells (0% cytotoxicity) and cells treated with 20 µM camptothecin (100% cytotoxicity).

3. Results

3.1. Development of a Reverse-Nanoluciferase (Rev-Nluc) reporter to monitor nsp5 activity

To develop a Nanoluciferase-based reporter for SARS-CoV-2 nsp5 activity, we built on our experience in engineering a split Nanoluciferase for protein complementation assays (Choi et al., 2019). We designed a Reverse-Nanoluciferase (Rev-Nluc-CoV, Fig. 1A) in which the two independent structural Nanoluciferase domains corresponding to amino acids 2–66 and 66–171 are permuted and separated by a flexible loop including the coronavirus nsp5 consensus cleavage site VRLQ/S (Kilianski et al., 2013). As a control, a TEV protease cleavage site or a sequence corresponding to two BsmBI restriction sites was inserted into the Rev-Nluc (Rev-Nluc-TEV and Rev-Nluc-control, respectively). To determine the efficiency of nsp5-mediated Rev-Nluc cleavage, the Rev-Nluc-CoV plasmid was co-transfected with a plasmid encoding nsp4, nsp5 and the amino-terminal part of nsp6 (O'Brien et al., 2021b). Previous studies have shown that nsp5 is released upon autocatalytic processing of the coronavirus nsp4-5-6 polyprotein (Kilianski et al., 2013; Muramatsu et al., 2016; O'Brien et al., 2021b). As a control, a catalytically inactive nsp5 mutant (C145A) was used (Muramatsu et al., 2016).

A luciferase signal was measured in cells co-transfected with the Rev-Nluc-CoV and a control empty plasmid, demonstrating that the permuted Nanoluciferase domains form an active enzyme. Compared to the empty vector control, cells co-transfected with the SARS-CoV-2 nsp4-5-6 WT plasmid showed a ~30-fold reduction in luciferase signal at 48 hpt, whereas Nanoluciferase signals in cells co-transfected with the
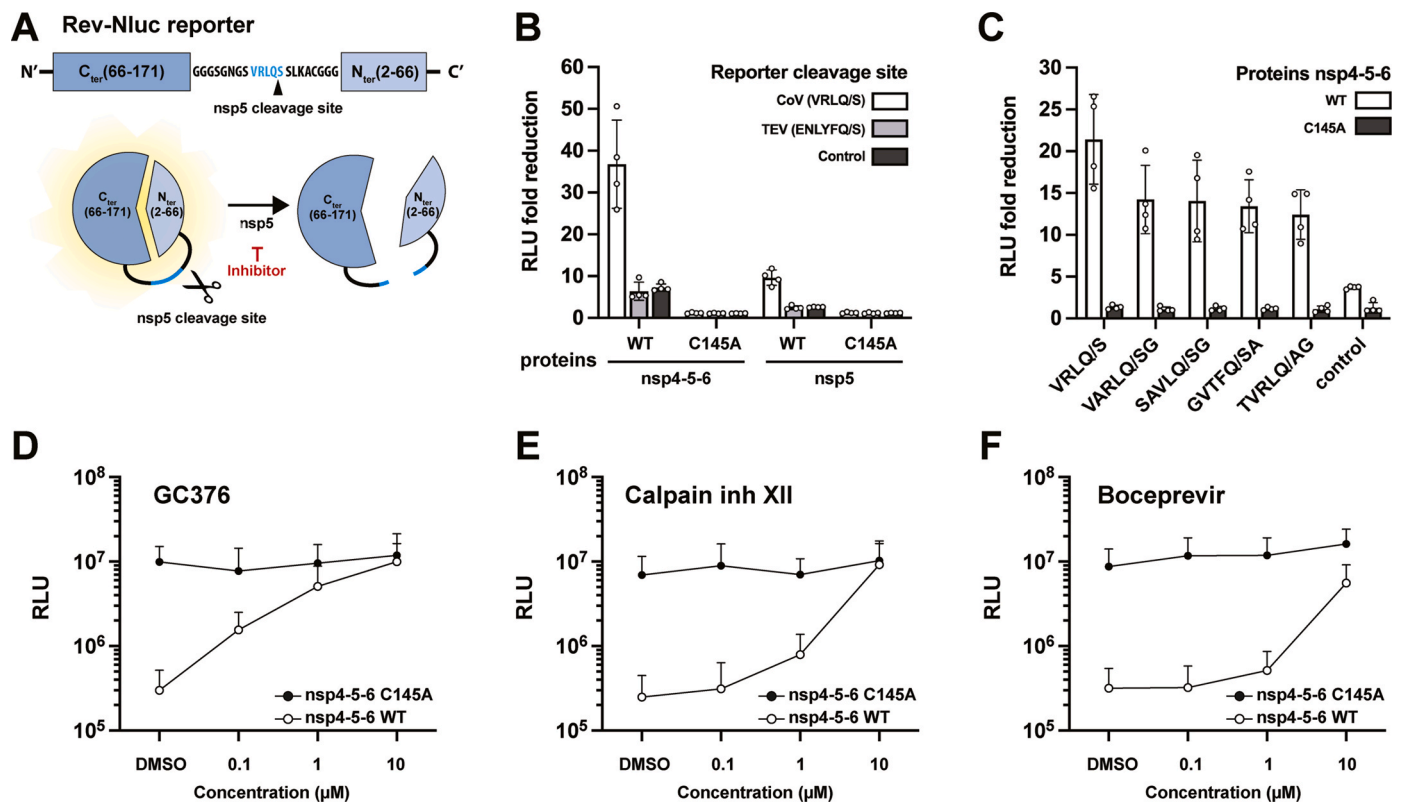
Fig. 1. Development of a Nanoluciferase-based reporter to monitor nsp5 activity. A. Schematic representation of the Rev-Nluc-CoV based assay for nsp5/3CLpro activity. The Rev-Nluc-CoV reporter was designed so that the N-terminal and C-terminal domains of the Nanoluciferase are permuted and separated by a flexible loop including the coronavirus nsp5 consensus cleavage site (VRLQ/S). Reporter cleavage by nsp5 reduces Nanoluciferase activity. Inhibition of nsp5 increases Nanoluciferase activity **B.** Luciferase signals measured at 48 hpt in HEK-293T cells transfected with a Rev-Nluc reporter (CoV cleavage site, TEV cleavage site or a control linker sequence) and nsp4-5-6 (WT or C145A) or nsp5 (WT or C145A). The graph shows the Relative Light Unit (RLU) fold reduction compared to cells transfected with an empty control plasmid instead of the nsp4-5-6 or nsp5 plasmid (mean ± SD of four independent experiments performed in technical triplicates). **C.** Luciferase signals measured at 24 hpt in HEK-293T cells transfected with a Rev-Nluc reporter (with different nsp5 cleavage sites or a control linker sequence), and nsp4-5-6 (WT or C145A). The graph shows the RLU fold reduction compared to cells transfected with an empty control plasmid instead of the nsp4-5-6 plasmid (mean ± SD of four independent experiments performed in technical triplicates). **D-F.** The inhibition of SARS-CoV-2 nsp5 by GC376 (D), Calpain Inhibitor XII (E) and Boceprevir (F) was assessed using the Rev-Nluc-based assay. The assay was performed as described in the Methods section. The RLU are shown as the mean ± SD of three independent experiments performed in technical triplicates. Open symbols: nsp4-5-6 WT; closed symbols: nsp4-5-6 C145A.

SARS-CoV-2 nsp4-5-6 C145A remained unchanged (Fig. 1B, white bars, and Supplemental Fig. 1). When the Rev-Nluc-TEV and Rev-Nluc-control plasmids were used instead of the Rev-Nluc-CoV reporter plasmid, cells co-transfected with nsp4-5-6 WT showed a ~5-fold decrease in luciferase signal (Fig. 1B, light and dark grey bars, respectively). These data indicate that upon autocatalytic processing of the SARS-CoV-2 nsp4-5-6 polyprotein, the released nsp5 restricts the production of an active Nanoluciferase, and it does so through two distinct mechanisms: 1) cleavage of the canonical nsp5 site VRLQ/S in the Rev-Nluc and 2) reduction of Nanoluciferase activity independent of the canonical cleavage site, possibly caused by nsp5-mediated cleavage of Rev-Nluc at other sites or indirectly by cleavage of cellular proteins. The cleavage of the reporter is strictly dependent on the protease activity of nsp5, as demonstrated by the nsp5 C145A mutant. When nsp5 was expressed alone instead of the nsp4-5-6 polyprotein, the observed fold-changes were lower (Fig. 1B).

An orthogonal assay was used to confirm that the reduction in luciferase signal was due to nsp5-mediated cleavage of the reporter. The Rev-Nluc-CoV reporter was fused to the 3xFLAG tag at its N-terminal end and cleavage was assessed by western-blot using an anti-FLAG antibody. As shown in Supplemental Fig. 2, the full-length Rev-Nluc-CoV protein could no longer be detected upon co-expression of the SARS-CoV-2 nsp4-5-6 WT, while its levels remained unchanged upon expression of the C145A mutant. Notably, the FLAG-tagged cleavage product with an expected size of 19 kD (compared to 30 kD for the

uncleaved Rev-Nluc) could not be detected either, suggesting that it is degraded upon cleavage.

3.1.1. Comparison of Rev-Nluc reporters with different nsp5 cleavage sites

In an attempt to optimize the Rev-Nluc reporter, we replaced the initial coronavirus nsp5 consensus VRLQ/S cleavage site by the VARLQ/SG sequence that was identified as an optimal SARS-CoV nsp5 cleavage site (Chuck et al., 2011), or by three nsp5 cleavage sites in the SARS-CoV-2 ORF1a at the nsp4-5 (SAVLQ/SG), nsp5-6 (GVTFQ/SA) and nsp9-10 (TVRLQ/AG) junctions. With all reporter plasmids, a decrease in luciferase signal was measured in cells expressing SARS-CoV-2 nsp4-5-6 WT (Fig. 1C, white bars) compared to the empty vector, but not in cells expressing the mutant SARS-CoV-2 nsp4-5-6 C145A (Fig. 1C, dark grey bars). The highest fold change was observed with the Rev-Nluc-CoV plasmid (VRLQ/S), which was used in the following experiments in combination with SARS-CoV-2 nsp4-5-6 WT or C145A.

3.1.2. Effect of nsp5 inhibition on Rev-Nluc activity

The fold-change in Nanoluciferase signal measured between the WT and C145A mutant is dependent on nsp5 enzymatic activity and can therefore be used as a proxy for *in vivo* nsp5 activity. To investigate whether the Rev-Nluc reporter could be used to screen for inhibitors of nsp5, we tested the commercially available GC376 compound that was reported to inhibit SARS-CoV-2 nsp5 activity *in vitro* (Fu et al., 2020; Ma et al., 2021) as well as in cell-based assays (Froggatt et al., 2020; Rawson

et al., 2021) and to inhibit SARS-CoV-2 replication in Vero cells (Hung et al., 2020). GC376 dose-dependently reduced nsp5 activity, as seen by a gradual increase of Nanoluciferase activity measured in the presence of SARS-CoV-2 nsp4-5-6 WT (Fig. 1D, open symbols), while the luciferase signal measured in the presence of catalytically inactive mutant remained unchanged (Fig. 1D, closed symbols). Full inhibition of nsp5 was achieved at 10 μM GC376 and the estimated IC_{50} was in the micromolar range, in agreement with previous findings in cell-based assays (Froggatt et al., 2020; Iketani et al., 2021; Vuong et al., 2020). The inhibitory effects of Calpain Inhibitor XII and Boceprevir as determined by the Rev-Nluc assay were lower compared to GC376 (Fig. 1E and F), consistent with the reported *in vitro* IC_{50} values (0.45 and 4.13 μM respectively, compared to 0.03 μM for GC376 in Ma et al., 2021).

3.1.3. Extended use of the Rev-Nluc assay

We asked whether the Rev-Nluc-CoV reporter can be used to monitor the activity of nsp5 proteins from distantly related coronaviruses. To this end, the Rev-Nluc-CoV plasmid was co-transfected with nsp5 expression vectors derived from SARS-CoV-2 (*Betacoronavirus*), the human seasonal coronavirus 229E (hCoV-229E, *Alphacoronavirus*) or the avian infectious bronchitis virus (IBV, *Gammacoronavirus*). Compared to the empty vector control, a 50- to 100-fold reduction was observed in the presence of SARS-CoV-2, hCoV-229E and IBV nsp5 (Fig. 2A). These findings are consistent with data obtained with a FlipGFP nsp5 reporter (Froggatt et al., 2020), and show that the Rev-Nluc assay can be adapted to other coronaviruses.

Next, we asked whether the Rev-Nluc reporter could be used to monitor the activity of a distinct class of proteases, the hepatitis C virus (HCV) NS3/4A serine protease. The Rev-Nluc-HCV reporter plasmid, in which the two Nanoluciferase subdomains are linked by the NS5A/5B cleavage site EDVVCCSMSY, was co-transfected with an expression vector for NS3/4A protease. Cells co-transfected with the NS3/4A plasmid showed a ~20-fold reduction in luciferase signal at 48 hpt, whereas luciferase signals in cells co-transfected with the catalytically inactive S139A mutant (Bartenschlager et al., 1993) showed no change (Fig. 2B, grey bars, and Supplemental Fig. 3). In the presence of two potent NS3/4A protease inhibitors (BI-1230 and BI-1388, Boehringer Ingelheim), a dose-dependent increase of the Nanoluciferase signal was observed in the presence of NS3/4A WT (open symbols) while the luciferase signal measured in the presence of NS3/4A S139A remained unchanged (closed symbols) (Fig. 2C–D). The estimated IC_{50} as measured by the Rev-Nluc assay was 0.02 μM, in the same range as previously reported (https://opnme.com/).

3.1.4. Implementation of an automated 384-well Rev-Nluc-assay pipeline

To allow the screening of large compound libraries with potential anti-nsp5 activity, we adapted the Rev-Nluc assay to the 384-well format in an automated pipeline as described in detail in the Methods section. In brief, HEK-293T cells are transfected in bulk, harvested at 6 hpt and distributed homogeneously in 384-well plates which contain pre-distributed compounds (Fig. 3A). This reduces transfection efficiency variations between wells and increases time- and cost-effectiveness. In a
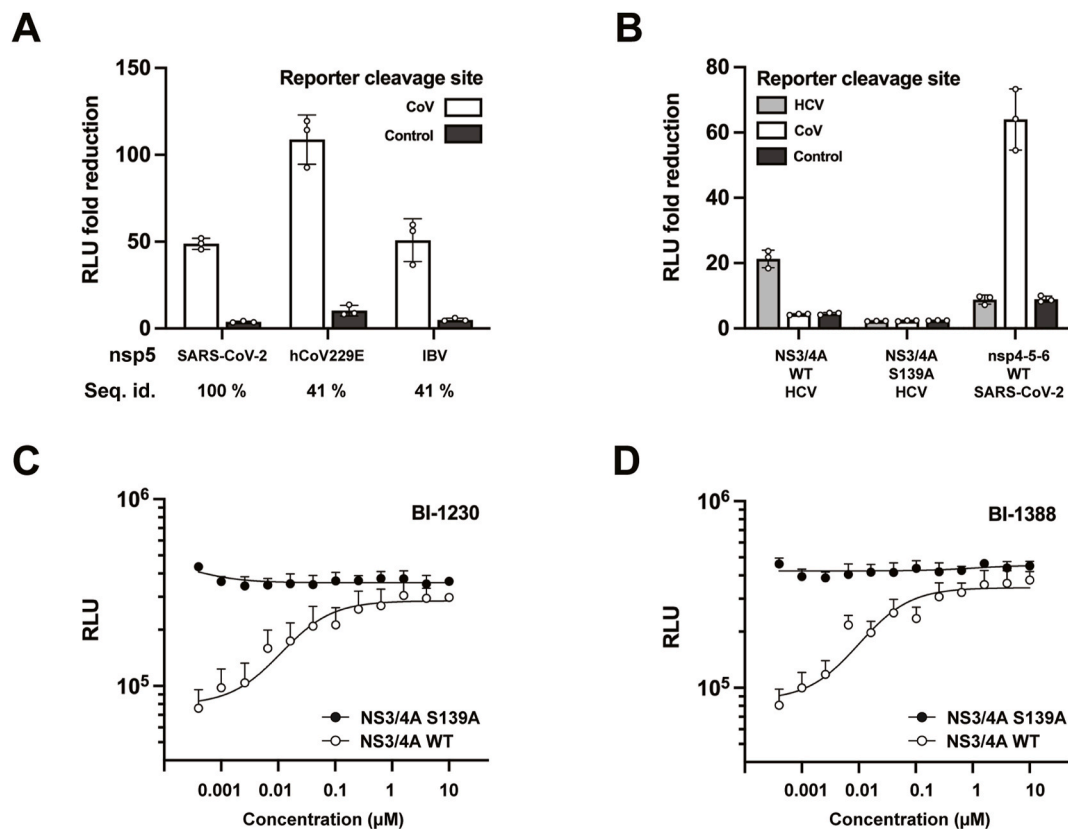

Fig. 2. Extended use of the Rev-Nluc assay. A. Luciferase signal measured at 48 hpt in HEK-293T cells co-transfected with a Rev-Nluc reporter (with a CoV or control linker sequence) and nsp5 (derived from SARS-CoV-2, hCoV-229E, or IBV). The graph shows the RLU fold-reduction compared to cells transfected with an empty control plasmid (mean ± SD of three independent experiments performed in technical triplicates). The amino acid sequence identity compared to SARS-CoV-2 nsp5 is indicated below the graph. **B.** Luciferase signal measured at 48 hpt in HEK-293T cells co-transfected with a Rev-Nluc reporter (with an HCV-NS5A/5B, a CoV cleavage site, or a control linker sequence) and HCV-NS3/4A protease (WT or S139A) or SARS-CoV-2 nsp4-5-6. The graph shows the RLU fold-reduction compared to cells transfected with an empty control plasmid instead of an NS3/4A or nsp4-5-6 plasmid (mean ± SD of three independent experiments performed in technical triplicates). **C-D.** The inhibition of HCV-NS3/4A protease by BI-1230 (C) and BI-1388 (D) at concentrations from 10 to 0.0004 μM was assessed using the Rev-Nluc-based assay. The RLU are shown as the mean ± SD of two independent experiments performed in technical triplicates. Open symbols: NS3/4A WT; closed symbols: NS3/4A-S139A.

A

B

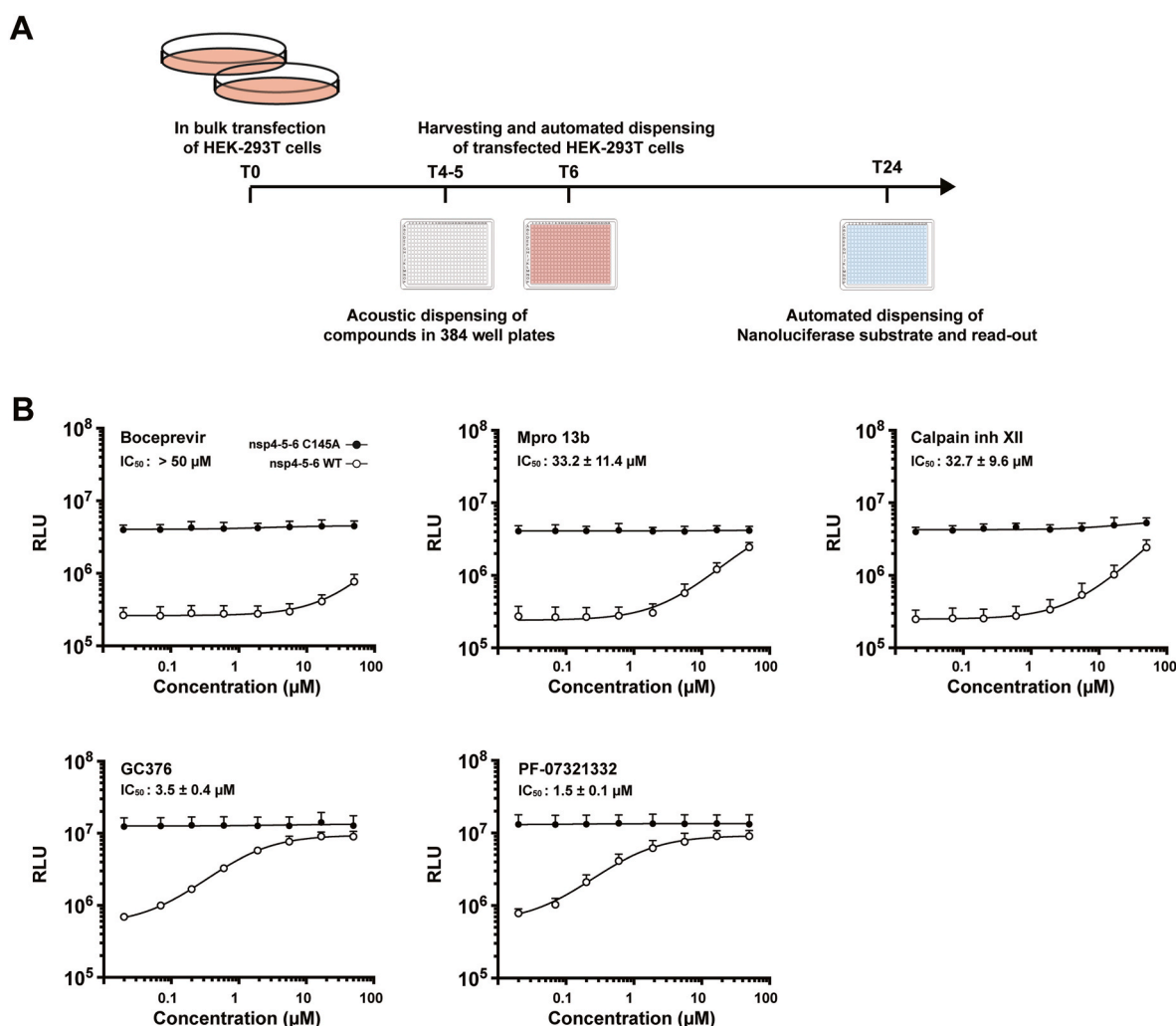**Fig. 3. Upscaling of the Rev-Nluc-based assay to the 384-well format. A.** Schematic representation of the automated high-throughput pipeline to perform the Rev-Nluc assay in a 384-well format. The initial point of the timeline (hours post-transfection) is indicated as T0. **B.** The inhibition of SARS-CoV-2 nsp5 by GC376, Mpro13b, Calpain Inhibitor XII, Boceprevir and PF-07321332 was assessed using the Rev-Nluc-based assay in a 384-well plate setting. Cells were transfected either with SARS-CoV-2 nsp4-5-6 WT (open symbols) or C145A (black symbols). Experiments with Boceprevir, Mpro 13b and Calpain Inhibitor XII were done with a different batch of cells than experiments with GC376 and PF-07321332. The inhibitor concentrations correspond to 3-fold serial-dilutions from 50 to 0.02 μM. The graphs show Relative Light Units (RLU) measured as described in the Methods section and expressed as the mean $\pm$ SD of two independent experiments, each performed in technical triplicates.

preliminary experiment, we assessed the reproducibility of the luciferase signal across ten 384-well plates with GC376 at final concentrations of 10, 1 or 0.1 μM. The luciferase signal distribution and relative nsp5-inhibition by GC376 remained stable throughout the series (Supplemental Fig. 4). The robustness of the assay was also demonstrated by a z'-factor of 0.8, which taken together with its miniaturisation and rapidity, makes it compatible with high-throughput use. When the same conditions were used to perform dose-response curves with GC376, Calpain Inhibitor XII, Boceprevir, the alpha-ketoamide inhibitor Mpro 13b, and the recently approved oral inhibitor PF-07321332, the relative levels of nsp5 inhibition and estimated IC_{50} values were consistent with previous reported *in vitro* activities (Hung et al., 2020; Ma et al., 2021; Owen et al., 2021; Rawson et al., 2021; Zhang et al., 2020) (Fig. 3B). Overall, our data demonstrate that the Rev-Nluc-based is scalable to the 384-well format and can be reliably used to screen large libraries for small molecule inhibitors of SARS-CoV-2 nsp5.

3.2. In silico-based selection of potential anti-nsp5 compounds

We used the available structural information on ligand-bound nsp5

proteins (98 covalent and 40 non-covalent crystallographic complexes) to derive a pharmacophore (Supplemental Methods section and Supplemental Fig. 5). Among the non-covalent complexes, 38 were bearing proper ligands to perform crossdocking experiments and were used as candidates to select for the most suitable docking protocol/schemes. The docking of an in-house library of 14,468 compounds was performed on the PDB entries 7JU7, 5R7Z and 5RH8 with the Smina software (Koes et al., 2013) and on PDB 5RH8 with the FlexX software (Rarey et al., 1996), as the combination of these four docking schemes gave the best results for crossdocking on the non-covalent crystallographic complexes (Supplemental Methods section). Molecules which could not be docked because they had unusual atoms, had too many rotatable bonds, or could not fit for other reasons were discarded. Out of the 14,468 compounds, 13,781 could be docked at least once for one of their ~60,000 tautomers/conformers. With up to 10 poses recorded, this led to ~2,400,000 poses. For each docking pose, a pharmacophoric score (named PHARMscore) was calculated as described in the Supplemental Methods section. Noticeably, comparison of the docking poses of FlexX and Smina on PDB 5RH8 showed better PHARMscore for FlexX. Correlations between the PHARM scores and rescoring values were significant for the

selected molecules (from 0 to 58%) ("Whole selection" in the Supplemental Table 1). The correlation was higher for the best rescored poses than for the best PHARM poses, suggesting that the rescoring considers the molecular contacts used to calculate the PHARMscores and is more exhaustive.

For each molecule and each docking scheme, the pose with the top score upon docking and the pose with the top PHARMscore were selected and were used for the selection/prioritization of molecules as described in the Supplemental Methods section. This led to 393, 381, 376, 310 unique poses (or 371, 307, 319 and 371 unique molecules) for 5R7Z-Smina-HYDE, 5RH8-FlexX, 5RH8-Smina-AD4 and 7JU7-Smina-AD4, respectively, representing a total of 1460 unique poses (or 933 unique molecules) that were further analysed (Supplemental Fig. 6). Noticeably, the following molecular interactions were observed most frequently (frequency in brackets): HBond:GLU166 (75%), Cation-π: HIS41 (46%), π-π:HIS41 (37%), HBond:GLY143 (30%), Tstack:HIS41 (27%), HBond:HIS163 (23%), SaltBridge:GLU166 (21%). In comparison, the most frequent interactions observed in the crystal complexes were HBond:GLU166 (37%), HBond:HIS163 (26%), Tstack:HIS41 (17%), HBond:GLY143 (8%). After visual inspection, 46, 121, 107 and

84 poses were selected from the 5R7Z-Smina-HYDE, 5RH8-FlexX, 5RH8-Smina-AD4 and 7JU7-Smina-AD4 docking models respectively, representing a list of 316 unique candidate molecules. An additional 23 molecules were selected because of their chemical similarity to control compounds (GC376, Calpain Inhibitor XII, Boceprevir and Masitinib), bringing to 339 the number of selected molecules (named *in silico Selection #1* below, in the Supplemental Table 1 and Table 1). A second filtering of the ~2,400,000 poses was performed based on features frequently observed both in available crystallographic complexes (Dai et al., 2020; Fu et al., 2020; Gunther et al., 2021; Jin et al., 2020; Lockbaum et al., 2021; Ma et al., 2020; Sacco et al., 2020; Su et al., 2020; Zhang et al., 2020) and in the poses of the *in silico Selection #1* (namely hydrogen bonds to residues 163 and 166 and pyridine, acetamide/urea moieties) and geometric/positional similarity to crystal complexes. The 1354 filtered poses, representing 1142 unique molecules, were visually inspected to select 20 additional molecules (named *in silico Selection #2*). In total, 359 molecules (*Selection #1* and *#2*) were selected for experimental testing.

Table 1
Primary and secondary screen of candidate nsp5 inhibitors.

Source	Docking Scheme	Compound name	Compound #	Predicted solubility	Primary screen nsp5-WT RLU (%) [a]	Secondary screen nsp5-WT RLU (%) [a]	nsp5-CA RLU (%) [b]
Target Mol		UNC2881	1		29.5	18.2 ± 0.5	295.3 ± 15.8
Target Mol		dBET6	2		17.3	15.2 ± 1.0	233.3 ± 6.6
Target Mol		Lacidipine	3		10.2	8.9 ± 0.7	121.2 ± 7.4
In Silico #1	5R8H-FlexX	Volasertib (BI6727)	4		83.9	114.5 ± 8.9	>250
In Silico #1	5R7Z-Smina	Merimepodib	5		46.1	38.6 ± 1.6	110.4 ± 10.8
In Silico #1	5R8H-FlexX	Fedratinib (SAR302503)	6		32.7	57.6 ± 8.6	>250
In Silico #1	5R8H-FlexX	OTX015	7	Low	31.8	31.5 ± 11.0	>250
In Silico #1	5R8H-FlexX	TG101209	8		30.0	34.9 ± 4.0	>250
In silico #1	7JU7-Smina	Pacritinib (SB1518)	9	Low	28.2	15.3 ± 1.3	98.3 ± 4.0
In silico #1	7JU7-Smina	AT9283	10		24.0	14.7 ± 0.8	71.3 ± 8.3
In silico #1	5RH8-Smina	Fr-PPIchem-33-E11_10265	11		22.8	14.0 ± 1.7	110.3 ± 9.1
In silico #1	7JU7-Smina	CP 673451	12		19.4	13.9 ± 0.9	144.6 ± 10.3
In silico #1	5RH8-Smina	Fr-PPIchem-18-N22_05720	13		18.8	19.2 ± 1.4	270.7 ± 1.7
In silico #1	5R8H-FlexX	Fr-PPIchem-05-G10_01408	14	Low	17.7	19.2 ± 1.0	148.3 ± 18.6
In silico #1	5R7Z-Smina	Fr-PPIchem-29-J4_09142	15		16.8	10.0 ± 1.4	168.3 ± 2.9
In silico #1	5RH8-FlexX	BMS-833923 (XL139)	16	Low	16.4	16.2 ± 2.1	256.0 ± 74.0
In silico #1	5RH8-Smina	SNS-032 (BMS-387032)	17		15.7	10.7 ± 1.1	66.6 ± 3.4
In silico #1	5R8H-FlexX	Fr-PPIchem-33-E19_10269	18		15.3	10.6 ± 2.4	207.0 ± 8.0
In silico #1	5R8H-FlexX	Fr-PPIchem-24-G17_07495	19		14.6	11.8 ± 1.3	72.0 ± 2.3
In silico #1	5RH8-Smina	Rociletinib (CO-1686. AVL-301)	20	Low	13.3	9.7 ± 1.9	181.9 ± 10.4
In silico #1	5R8H-FlexX	Dasatinib (BMS-354825)	21		11.6	10.7 ± 1.7	249.1 ± 19.9
In silico #1	5RH8-FlexX	Fr-PPIchem-08-N15_02513	22	Low	10.8	8.4 ± 0.7	107.0 ± 3.0
In silico #1	5RH8-Smina	Osimertinib (AZD9291)	23		10.1	8.3 ± 2.3	43.2 ± 6.7
In silico #1	5R8H-FlexX	Fr-PPIchem-27-O18_08616	24	Low	9.8	9.0 ± 0.5	116.0 ± 5.6
In silico #2	5R8H-FlexX	Fr-PPIchem-33-M5_10302	25		nd	1.5 ± 0.4	110.3 ± 6.7
In silico #2	5R8H-FlexX	Fr-PPIchem-28-C12_08690	26		nd	1.2 ± 0.4	97.7 ± 3.6
In silico #2	5R8H-FlexX	Fr-PPIchem-25-K5_07883	27		nd	1.1 ± 0.6	94.9 ± 3.2
In silico #2	5R8H-FlexX	Fr-PPIchem-25-H16_07834	28		nd	2.8 ± 1.4	103.1 ± 9.9
In silico #2	5R8H-FlexX	Fr-PPIchem-25-H14_07832	29		nd	0.7 ± 1.0	98.3 ± 3.0
In silico #2	7JU7-Smina	Fr-PPIchem-24-K10_07568	30	Low	nd	5.1 ± 0.8	129.3 ± 3.5
In silico #2	5R8H-Smina	Fr-PPIchem-24-J10_07548	31		nd	1.2 ± 0.2	96.9 ± 6.6
In silico #2	5R8H-FlexX	Fr-PPIchem-23-J19_07237	32		nd	1.2 ± 0.8	89.6 ± 0.6
In silico #2	5R8H-FlexX	Fr-PPIchem-23-E18_07136	33	Low	nd	3.0 ± 0.6	110.0 ± 7.0
In silico #2	5R8H-FlexX	Fr-PPIchem-20-F19_06197	34	Low	nd	1.6 ± 0.3	110.7 ± 8.1
In silico #2	5R8H-FlexX	Fr-PPIchem-20-D4_06142	35	Low	nd	49.9 ± 0.2	113.3 ± 4.7
In silico #2	5R8H-FlexX	Fr-PPIchem-17-B10_05148	36		nd	0.4 ± 0.4	97.5 ± 6.1
In silico #2	5R8H-FlexX	Fr-PPIchem-10-O14_03172	37	Low	nd	2.4 ± 0.9	104.1 ± 8.0
In silico #2	5R8H-FlexX	Fr-PPIchem-09-G14_02692	38	Low	nd	9.7 ± 1.3	134.3 ± 7.0
In silico #2	5R8H-Smina	Fr-PPIchem-08-H7_02385	39	Low	nd	7.9 ± 2.7	106.3 ± 10.7
In silico #2	5R8H-Smina	Fr-PPIchem-05-K6_01484	40	Low	nd	2.8 ± 1.7	107.0 ± 6.0
In silico #2	5R8H-Smina	Fr-PPIchem-03-O22_00940	41		nd	0.9 ± 0.4	92.3 ± 7.6
In silico #2	5R8H-Smina	Fr-PPIchem-03-H4_00782	42		nd	0.6 ± 0.5	84.3 ± 3.7
In silico #2	5R8H-FlexX	Rebamipide	43		nd	−1.5 ± 0.5	71.6 ± 6.5
In silico #2	5R8H-FlexX	Metyrapone	44		nd	−1.4 ± 0.2	77.7 ± 2.4

[a] percent of [GC376 50 μM].
[b] percent of [DMSO 0.5%].

3.3. Screening of candidate nsp5 inhibitors

We applied the 384-well Rev-Nluc-assay pipeline to test the 339 candidate nsp5 inhibitors corresponding to the *in silico Selection #1*. In parallel, we also tested a commercial (TargetMol) library of 161 small molecules with potential anti-nsp5 activity as predicted by molecular docking. In a primary screen, the compounds were distributed into 384-well plates at final concentrations of 10 μM. The luciferase signals were background subtracted and expressed as percentages of the mean signal of cells treated with the control compound GC376 (50 μM). Nsp5 inhibition of the 500 tested compounds was ranked by their potency from left to right, and the compounds showing a luciferase signal ≥10% of the signal measured in the presence of 50 μM GC376 are represented in blue (Fig. 4A). Among those, 3 belong to the TargetMol library and 21 to the *in silico Selection #1* (Table 1, compounds #1 to #24).

To assess the specificity of nsp5 inhibition and potential cell toxicity, the 24 primary hit compounds were tested at a final concentration of 10 μM in cells transfected with either SARS-CoV-2 nsp4-5-6 WT or C145A. Compounds that led to an increased (>120%) or decreased (<80%) luciferase signal in SARS-CoV-2 nsp4-5-6 C145A-transfected cells were discarded. The 5 remaining compounds (# 5, 9, 11, 22 and 24, Table 1) induced a moderate to strong increase in luciferase signal with nsp5-WT, consistent with the primary screening data. The strongest increase (39% compared to the 50 μM GC376 control) was observed with compound #5. The twenty *in silico Selection #2* compounds were tested in the same conditions as the 24 primary hits and assessed using the same criteria, which led to the selection of two additional compounds (#35 and #39 in Table 1).

Dose-response curves were generated for the 7 secondary hit compounds on cells expressing either nsp5 WT or the nsp5 C145A mutant. Compound #9 (Pacritinib) showed a dose-response curve with an irregular pattern (Supp Fig. 7A) and was not further considered. The IC_{50} was estimated >50 μM for compounds #11 (Fr-PPIChem-33-E11_10265) and #22 (Fr-PPIChem-08-N15_02513) (Supp Fig. 7B–C, left panels), and <50 μM for compounds #5 (Merimepodib), #24 (Fr-PPI-Chem-27-O18_08616), #35 (Fr-PPIChem-20-D4_06142) and #39 (Fr-PPIChem-08-H7_02385) (Fig. 4B–E, left panels). Some compounds became toxic at 50 μM, as indicated by a sharp decrease of the luciferase signal both on the WT and mutant nsp5 (Fig. 4B, D and E, open and close symbols, respectively). Dose-response curves were then generated using an *in vitro* assay with the purified SARS-CoV-2 nsp5 protein, and concentration of compounds ranging from 0.5 to 600 μM. Because differences in the cell permeability and toxicity of compounds will have an impact in the cell-based but no the *in vitro* assay, a strong correlation between the activities observed in these two assays is not necessarily expected. Notably however, among the four most promising hits in the cell based assay, two compounds showed the lowest IC_{50} *in vitro* (#24 and #39, 74 ± 22 and 18 ± 4 μM, respectively) (Fig. 4C and E, right panels). Three compounds (#11, #22 and #35) showed IC_{50} values in the 140–150 μM range (Supp Fig. 7B and C and Fig. 4D, right panels), while compound #5 had an estimated IC_{50} > 600 μM (Fig. 4B, right panel). The high proportion of active compounds *in vitro* (5 out of 6 confirmed cellular hits) provides strong evidence that our cell-based assay can reliably identify *bona fide* nsp5 inhibitors. Possible explanations for the low *in vitro* activity of compound #5 are discussed below.

3.4. Antiviral activity of candidate nsp5 inhibitors

The ability of compounds #5, #24, #35 and #39 (whose structure is shown in Fig. 5A) to inhibit SARS-CoV-2 replication was evaluated in a multicycle replication assay on A549-ACE2 cells, followed by RT-qPCR quantification of the viral genomic RNA in the supernatant collected at 72 hpi (Fig. 5B, open symbols). Cytotoxicity of the compounds was assessed in parallel using the same concentrations ranging from 0.02 to 50 μM, and an assay based on ATP quantification (Fig. 5B, closed symbols). For the positive control GC376 we determined an EC_{50} of 14.7 μM

and a EC_{50} to CC_{50} ratio (selectivity index or SI) > 3. Merimepodib (#5) showed an EC_{50} of 21 μM and a low SI of 1.5. Compounds #35, #24 and #39 showed EC_{50}s of 12.4, 7.2 and 4.7 μM, respectively, in line with the IC_{50} values determined in the *in vitro* protease activity assay (140, 74 and 18 μM, respectively). The lower EC_{50}s values in the cellular antiviral assay can possibly result from intracellular hydrolysis of these compounds into more active derivatives, or from a dual inhibition of nsp5 together with other viral or cellular protein(s). In summary, the screening of 520 candidate SARS-CoV-2 nsp5 inhibitors by the here described assay led to the identification of 2 potential lead compounds (#24, #39) with low cell toxicity up to 50 μM (SI > 7 and > 10, respectively) and a higher antiviral activity against SARS-CoV-2 replication as compared to the reference compound GC376, which demonstrates the potential of the Rev-Nluc assay for the identification of novel SARS-CoV-2 nsp5 inhibitors.

4. Discussion

We developed and validated a sensitive, high-throughput cell-based assay to monitor SARS-CoV-2 nsp5 proteolytic activity. We used this cell-based assay to screen a total of 520 candidate molecules for their ability to inhibit SARS-CoV-2 nsp5 activity, and identified two novel lead compounds. This was achieved by engineering a Reverse-Nanoluciferase (Rev-Nluc) reporter in which two Nanoluciferase domains are permuted and linked together by an nsp5 cleavage site. Co-expression with the SARS-CoV-2 nsp4-5-6 polyprotein results in cleavage of the reporter and thereby a significant reduction in luciferase activity. The addition of a specific nsp5 inhibitor results in a dose-dependent restoration in luciferase activity. A ~30-fold increase in luciferase activity is observed in the presence of 50 μM GC376, similar to the level of luciferase activity observed when a control inactive nsp4-5-6 polyprotein is co-expressed with the reporter instead of the wild-type nsp4-5-6. The strengths of the Rev-Nluc-based assay lie in the following: i) it is a gain-of-signal assay and therefore excludes compounds that are cytotoxic or interfere negatively with the Nanoluciferase read-out; ii) it is rapid and convenient due to the glow-type signal of the Nanoluciferase; iii) it is amenable to miniaturisation due to the very bright luminescence signal produced by the Nanoluciferase; and iv) as a consequence of its rapidity and miniaturisation it can be run in parallel on a wild-type and a catalytically inactive nsp5, which allows for the identification of compounds that restore the luciferase activity in both conditions and to discard them as false-positives. Unlike previously described SARS-CoV-2 nsp5 reporter assays, we provide evidence that our Rev-Nluc-based assay is scalable for high-throughput screens in a 384-well format.

The first cell-based assays for SARS-CoV-2 nsp5 to be described were loss-of-signal assays based on a Flip-GFP (Froggatt et al., 2020) or a Flip-Firefly (O'Brien et al., 2021b) reporter. They are less scalable for high-throughput application than the Rev-Nluc-based assay because of the low intensity and narrow dynamic range of fluorescence signals, or the flash-type signal of the Firefly luciferase. To date, two gain-of-signal assays were described. The first assay uses crystal violet staining as a read-out to monitor cytotoxicity upon nsp5 overexpression and is therefore not specific for nsp5 protease inhibition, as reduced cytotoxicity may result from off-target effects of the compounds (Resnick et al., 2021). More recently Rawson et al. described a gain-of-signal assay (Rawson et al., 2021), which differs from ours in that it is based on the NanoBiT system (Dixon et al., 2016). The two Nanoluciferase-derived domains which are linked together by an nsp5 cleavage site are more unbalanced in size (156 and 13 amino acids, compared to 105 and 61 for Rev-Nluc) and together they show 15 amino acid substitutions compared to the Rev-Nluc sequence. The ability of the NanoBiT-based assay to identify nsp5 inhibitors was demonstrated in a 96-well format, however its performance in terms of stability and scalability for a high-throughput screens was not investigated (Rawson et al., 2021).
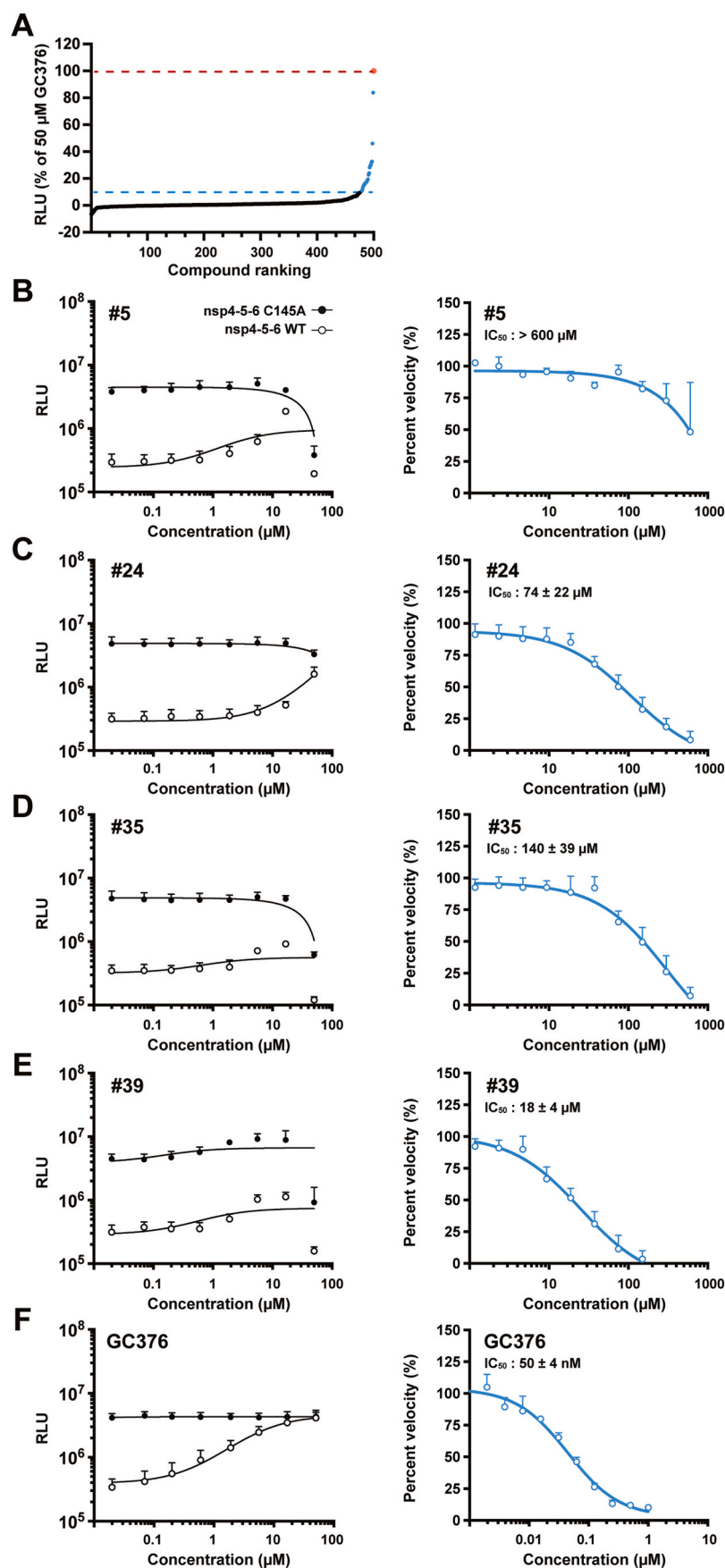
Fig. 4. Identification of nsp5 inhibitors using the cell-based Rev-Nluc assay and the *in vitro* FRET-based assay. A. Rev-Nluc-based primary screening of 500 putative nsp5 inhibitors. The 339 compounds from the *in silico Selection #1* and 161 compounds from the TargetMol nsp5-targeted library were distributed into 384-well plates to achieve final concentrations of 10 μM upon addition of cells transfected with SARS-CoV-2 nsp4-5-6-WT. The graphs show Relative Light Units (RLU) normalized as described in the methods section. Compounds are ranked according to the observed increase in luciferase signal from left to right, and the primary hits (≥10% luciferase signal compared to 50 μM GC376) are indicated in blue color. **B–F.** Analysis of secondary hits. Compounds #5 (B), #24 (C), #35 (D) and #39 (E) were tested at various concentrations in the Rev-Nluc assay and in the FRET-based *in vitro* assay using purified nsp5 protein. The GC376 compound was used as a control (F). For the cell-based assay (left panels), compounds were distributed into 384-well plates to achieve final concentrations of 50 to 0.02 μM upon addition of cells expressing either SARS-CoV-2 nsp4-5-6 WT (open symbols) or C145A (black symbols). The graphs show RLU measured as described in the methods section (mean ± SD of two independent experiments, each performed in technical triplicates). For the FRET-based *in vitro* assay (right panels), 2-fold serial dilutions of the compounds from 600 to 1.2 μM were tested as described in the Methods section. The graphs show percent velocity compared to the DMSO control (mean ± SD of three (B, F) or five (C, D and E) independent experiments).
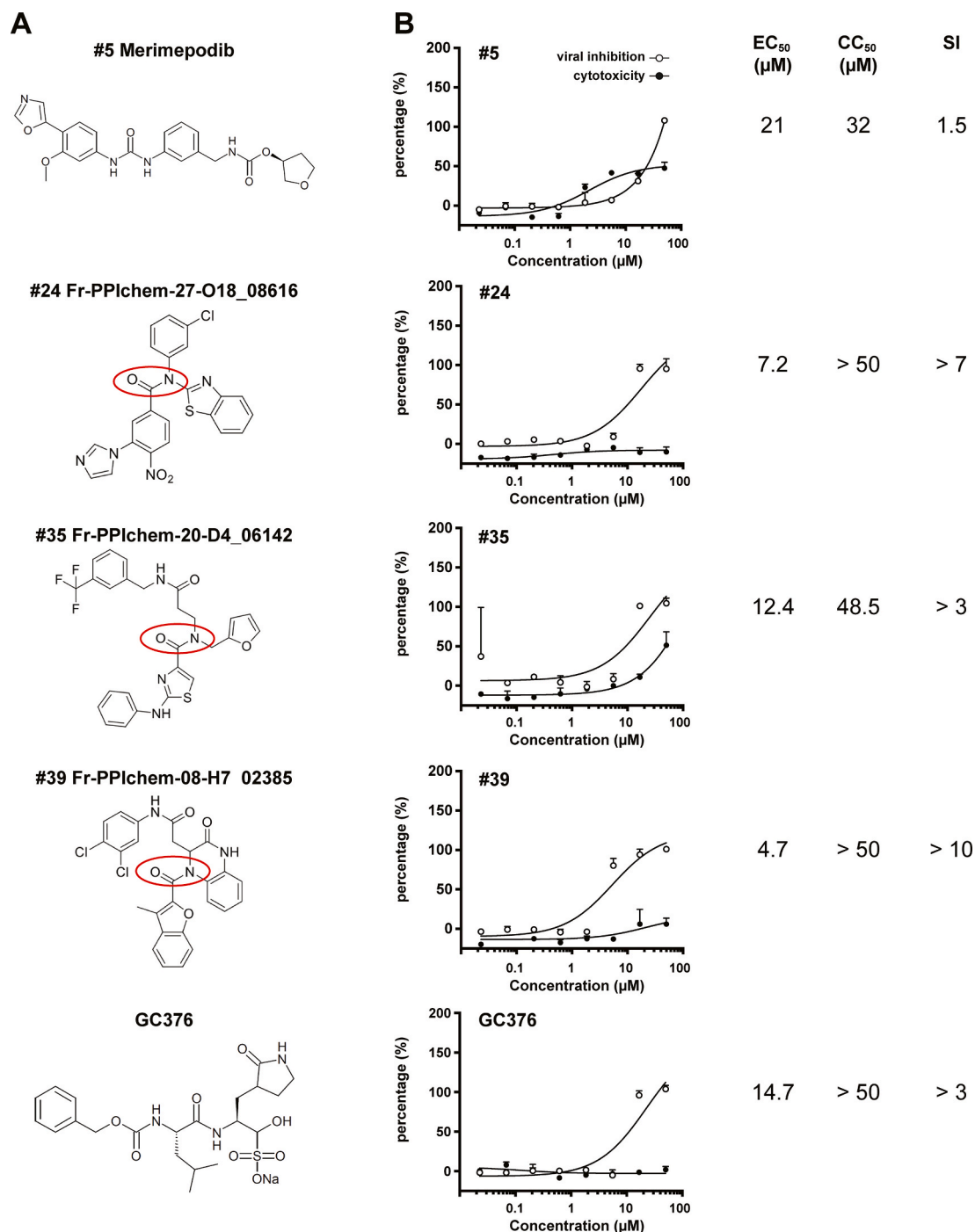
Fig. 5. Antiviral activity and cytotoxicity of nsp5 inhibitor candidates. A. The structure of the four secondary hit compounds (#5, #24, #35 and #39) is shown and their tertiary amide component is circled. GC376 was used as a control. **B.** The ability of compounds #5, #24, #35 and #39 to inhibit SARS-CoV-2 replication was evaluated at concentrations corresponding to 3-fold serial-dilutions from 50 to 0.02 μM in a multicycle replication assay on A549-ACE2 cells, followed by RT-qPCR quantification of the viral genomic RNA in the supernatant collected at 72 hpi. In parallel the indicated compounds were tested on A549-ACE2 cells for cell cytotoxicity with the CellTiter-Glo assay. The percent of viral inhibition (open symbols, mean ± SD of technical triplicates) and percent of cytotoxicity (closed symbols, mean ± SD of technical triplicates) were determined as described in the Methods section. One experiment representative of two independent experiments is shown.

We scaled-up the Rev-Nluc assay to an automated 384-well format, and used these conditions to assess the inhibition of SARS-CoV-2 nsp5 by a set of reference compounds: GC376, Boceprevir and Calpain Inhibitor XII, which have been shown to inhibit nsp5 and to impair viral replication (e.g. Fu et al., 2020; Hung et al., 2020; Ma et al., 2021; Sacco et al., 2020; Vuong et al., 2020), the alpha-ketoamide inhibitor 13b (Zhang et al., 2020), and the recently approved oral inhibitor PF-07321332 (Hammond et al., 2022; Owen et al., 2021). Our findings and IC50 estimations (Fig. 3B) were consistent with reported *in vitro* activities (Ma et al., 2021; Owen et al., 2021; Rawson et al., 2021; Zhang et al., 2020), therefore validating our assay.

We screened a total of 520 molecules with potential anti-nsp5 activity as predicted by molecular docking: 359 molecules from the *in silico* screening approach and 161 molecules from a commercial targeted

library. A primary screen, performed at a single concentration on the wild-type nsp5 protein only, identified 24 hits. The subsequent secondary screen, performed at a single concentration on the wild-type and catalytically inactive nsp5 proteins in parallel, led us to discard most of the primary hits as being toxic or false-positives and to select only 7 molecules, all coming from the *in silico* screening approach. Five out of these 7 selected molecules were found to inhibit purified nsp5 protease activity *in vitro*, with IC_{50} values ranging from 18 to 152 μM. These results highlight the fact that being able to manage parallel screening on the wild-type and catalytically inactive nsp5 proteins provides a major added value to our assay in terms of selectivity. Moreover, the fairly high hit rate of 5 hits out of 359 molecules indicates the effectiveness of the *in silico* screening approach, characterized by i) a careful selection of the available nsp5 structures to be used for docking, ii) a special attention paid to the *in silico* preparation of ligands for docking, iii) a comparison of several docking protocols, iv) the complementary use of a pharmacophoric score based on available structural information, and v) a meticulous analysis of the poses.

Upon dose-response analysis of the 7 selected hits, 4 molecules showed an estimated IC_{50} below 50 μM in the Rev-Nluc assay and were therefore assessed in a multicycle SARS-CoV-2 replication- and a cytotoxicity-assay. These molecules include merimepodib/VX-497, an inhibitor of the human inosine monophosphate dehydrogenase initially developed as an immunosuppressor (Jain et al., 2001). Merimepodib was later found to have antiviral activity against several DNA and RNA viruses including HCV, Zika, Ebola and FMDV viruses (Li et al., 2019; Marcellin et al., 2007; Markland et al., 2000; Tong et al., 2018). In the early phase of the COVID-19 pandemic, oral merimepodib was investigated in combination with intravenous remdesivir administration in a phase 2 clinical trial as a potential treatment for severe COVID-19. The trial sponsor announced in October 2020 that the trial was discontinued because it was unlikely that it would meet its primary safety endpoints (ViralClear Press release, 2020). Intriguingly, we found that merimepodib inhibits SARS-CoV-2 replication on A549-ACE2 cells with an EC_{50} of 21 μM and inhibits SARS-CoV-2 nsp5 protease activity in 293T cells with an $IC_{50} < 50$ μM, whereas it does not efficiently inhibit nsp5 protease activity *in vitro*. Merimepodib is unlikely to be a false-positive in the Rev-Nluc assay as it has a much stronger effect in the presence of the wild-type nsp5 compared to the catalytically inactive nsp5. Our observations are more likely explained by a different conformation of nsp5 and a higher accessibility of merimepodib binding site in the cellular context, or by an indirect mechanism of inhibition. Therefore, our data suggest a particular and unexpected mode of action of this compound against the SARS-CoV-2 virus. Merimepodib is thought to exert its broad antiviral activity by reducing the pool of intracellular guanine nucleotides and thereby impairing RNA and DNA synthesis. The question whether merimepodib can inhibit other viral cysteine-dependent proteases and to what extent this anti-protease activity contributes to its antiviral activity deserves to be further explored.

We also identified two compounds (#24 and #39 in Table 1 and Fig. 5) which inhibit SARS-CoV-2 replication on A549-ACE2 cells more efficiently than GC376, with IC_{50} values in the 4–8 μM range and selectivity indexes between 7 and 10. It was recently reported that cationic amphiphilic drugs (CAD) induce a phospholipidosis that can be confused with an antiviral effect (Tummino et al., 2021). Given its chemical structure, compound #39 cannot protonate and become cationic. Compound #24 can protonate with an estimated pKa value of 5.95, and is therefore predicted to be present mostly in its neutral form at physiological pH. Moreover the clogP values of compounds #24 and #39 are 5.72 and 5.03, respectively. Hence, it is very unlikely that these two molecules have a counfounding CAD-like activity. Both compounds #24 and #39 are components of the Fr-PPI-Chem library of putative protein-protein interaction inhibitors (Bosc et al., 2020). Interestingly, we note that they share a common tertiary amide component (circled in red on the structures shown in Fig. 5A), also present in compound #35 as well as in series of amides reported to inhibit the SARS-CoV nsp5

protease (Jacobs et al., 2013; Lockbaum et al., 2021; Turlington et al., 2013). Further experiments, including X-ray crystallography and biochemistry, will be needed to investigate the functional importance of this tertiary amide component, and to further assess the potential of these two compounds as starting points for the design of more effective nsp5 inhibitors.

Appendix A. Supplementary data

Supplementary data to this article can be found online at https://doi.org/10.1016/j.antiviral.2022.105272.

References

Bartenschlager, R., Ahlborn-Laake, L., Mous, J., Jacobsen, H., 1993. Nonstructural protein 3 of the hepatitis C virus encodes a serine-type proteinase required for cleavage at the NS3/4 and NS4/5 junctions. J. Virol. 67, 3835–3844.

Beigel, J.H., Tomashek, K.M., Dodd, L.E., Mehta, A.K., Zingman, B.S., Kalil, A.C., Hohmann, E., Chu, H.Y., Luetkemeyer, A., Kline, S., Lopez de Castilla, D., Finberg, R.W., Dierberg, K., Tapson, V., Hsieh, L., Patterson, T.F., Paredes, R., Sweeney, D.A., Short, W.R., Touloumi, G., Lye, D.C., Ohmagari, N., Oh, M.D., Ruiz-Palacios, G.M., Benfield, T., Fatkenheuer, G., Kortepeter, M.G., Atmar, R.L., Creech, C.B., Lundgren, J., Babiker, A.G., Pett, S., Neaton, J.D., Burgess, T.H., Bonnett, T., Green, M., Makowski, M., Osinusi, A., Nayak, S., Lane, H.C., Members, A.-S.G., 2020. Remdesivir for the treatment of covid-19 - final report. N. Engl. J. Med. 383, 1813–1826.

Berman, H.M., Westbrook, J., Feng, Z., Gilliland, G., Bhat, T.N., Weissig, H., Shindyalov, I.N., Bourne, P.E., 2000. The protein Data Bank. Nucleic Acids Res. 28, 235–242.

Boras, B., Jones, R.M., Anson, B.J., Arenson, D., Aschenbrenner, L., Bakowski, M.A., Beutler, N., Binder, J., Chen, E., Eng, H., Hammond, H., Hammond, J., Haupt, R.E., Hoffman, R., Kadar, E.P., Kania, R., Kimoto, E., Kirkpatrick, M.G., Lanyon, L., Lendy, E.K., Lillis, J.R., Logue, J., Luthra, S.A., Ma, C., Mason, S.W., McGrath, M.E., Noell, S., Obach, R.S., Mn, O.B., O'Connor, R., Ogilvie, K., Owen, D., Pettersson, M., Reese, M.R., Rogers, T.F., Rosales, R., Rossulek, M.I., Sathish, J.G., Shirai, N., Steppan, C., Ticehurst, M., Updyke, L.W., Weston, S., Zhu, Y., White, K.M., Garcia-Sastre, A., Wang, J., Chatterjee, A.K., Mesecar, A.D., Frieman, M.B., Anderson, A.S.,

Allerton, C., 2021. Preclinical characterization of an intravenous coronavirus 3CL protease inhibitor for the potential treatment of COVID19. Nat. Commun. 12, 6055.

Bosc, N., Muller, C., Hoffer, L., Lagorce, D., Bourg, S., Derviaux, C., Gourdel, M.E., Rain, J.C., Miller, T.W., Villoutreix, B.O., Miteva, M.A., Bonnet, P., Morelli, X., Sperandio, O., Roche, P., 2020. Fr-PPIChem: an academic compound library dedicated to protein-protein interactions. ACS Chem. Biol. 15, 1566–1574.

Cao, B., Wang, Y., Wen, D., Liu, W., Wang, J., Fan, G., Ruan, L., Song, B., Cai, Y., Wei, M., Li, X., Xia, J., Chen, N., Xiang, J., Yu, T., Bai, T., Xie, X., Zhang, L., Li, C., Yuan, Y., Chen, H., Li, H., Huang, H., Tu, S., Gong, F., Liu, Y., Wei, Y., Dong, C., Zhou, F., Gu, X., Xu, J., Liu, Z., Zhang, Y., Li, H., Shang, L., Wang, K., Li, K., Zhou, X., Dong, X., Qu, Z., Lu, S., Hu, X., Ruan, S., Luo, S., Wu, J., Peng, L., Cheng, F., Pan, L., Zou, J., Jia, C., Wang, J., Liu, X., Wang, S., Wu, X., Ge, Q., He, J., Zhan, H., Qiu, F., Guo, L., Huang, C., Jaki, T., Hayden, F.G., Horby, P.W., Zhang, D., Wang, C., 2020. A trial of lopinavir-ritonavir in adults hospitalized with severe covid-19. N. Engl. J. Med. 382, 1787–1799.

Choi, S.G., Olivet, J., Cassonnet, P., Vidalain, P.O., Luck, K., Lambourne, L., Spirohn, K., Lemmens, I., Dos Santos, M., Demeret, C., Jones, L., Rangarajan, S., Bian, W., Coutant, E.P., Janin, Y.L., van der Werf, S., Trepte, P., Wanker, E.E., De Las Rivas, J., Tavernier, J., Twizere, J.C., Hao, T., Hill, D.E., Vidal, M., Calderwood, M.A., Jacob, Y., 2019. Maximizing binary interactome mapping with a minimal number of assays. Nat. Commun. 10, 3907.

Chuck, C.P., Chow, H.F., Wan, D.C., Wong, K.B., 2011. Profiling of substrate specificities of 3C-like proteases from group 1, 2a, 2b, and 3 coronaviruses. PLoS One 6, e27228.

Dai, W., Zhang, B., Jiang, X.M., Su, H., Li, J., Zhao, Y., Xie, X., Jin, Z., Peng, J., Liu, F., Li, C., Li, Y., Bai, F., Wang, H., Cheng, X., Cen, X., Hu, S., Yang, X., Wang, J., Liu, X., Xiao, G., Jiang, H., Rao, Z., Zhang, L.K., Xu, Y., Yang, H., Liu, H., 2020. Structure-based design of antiviral drug candidates targeting the SARS-CoV-2 main protease. Science 368, 1331–1335.

Dixon, A.S., Schwinn, M.K., Hall, M.P., Zimmerman, K., Otto, P., Lubben, T.H., Butler, B.L., Binkowski, B.F., Machleidt, T., Kirkland, T.A., Wood, M.G., Eggers, C.T., Encell, L.P., Wood, K.V., 2016. NanoLuc complementation reporter optimized for accurate measurement of protein interactions in cells. ACS Chem. Biol. 11, 400–408.

Drayman, N., DeMarco, J.K., Jones, K.A., Azizi, S.A., Froggatt, H.M., Tan, K., Maltseva, N.I., Chen, S., Nicolaescu, V., Dvorkin, S., Furlong, K., Kathayat, R.S., Firpo, M.R., Mastrodomenico, V., Bruce, E.A., Schmidt, M.M., Jedrzejczak, R., Munoz-Alia, M.A., Schuster, B., Nair, V., Han, K.Y., O'Brien, A., Tomatsidou, A., Meyer, B., Vignuzzi, M., Missiakas, D., Botten, J.W., Brooke, C.B., Lee, H., Baker, S.C., Mounce, B.C., Heaton, N.S., Severson, W.E., Palmer, K.E., Dickinson, B.C., Joachimiak, A., Randall, G., Tay, S., 2021. Masitinib is a broad coronavirus 3CL inhibitor that blocks replication of SARS-CoV-2. Science 373, 931–936.

Fischer 2nd, W.A., Eron Jr., J.J., Holman, W., Cohen, M.S., Fang, L., Szewczyk, L.J., Sheahan, T.P., Baric, R., Mollan, K.R., Wolfe, C.R., Duke, E.R., Azizad, M.M., Borroto-Esoda, K., Wohl, D.A., Coombs, R.W., James Loftis, A., Alabanza, P., Lipansky, F., Painter, W.P., 2022. A phase 2a clinical trial of molnupiravir in patients with COVID-19 shows accelerated SARS-CoV-2 RNA clearance and elimination of infectious virus. Sci. Transl. Med. 14, eabl7430.

Froggatt, H.M., Heaton, B.E., Heaton, N.S., 2020. Development of a fluorescence-based, high-throughput SARS-CoV-2 3CL(pro) reporter assay. J. Virol. 94, e01265–20.

Fu, L., Ye, F., Feng, Y., Yu, F., Wang, Q., Wu, Y., Zhao, C., Sun, H., Huang, B., Niu, P., Song, H., Shi, Y., Li, X., Tan, W., Qi, J., Gao, G.F., 2020. Both Boceprevir and GC376 efficaciously inhibit SARS-CoV-2 by targeting its main protease. Nat. Commun. 11, 4417.

Gao, K., Wang, R., Chen, J., Tepe, J.J., Huang, F., Wei, G.W., 2021. Perspectives on SARS-CoV-2 main protease inhibitors. J. Med. Chem. 64, 16922–16955.

Group, R.C., Horby, P., Lim, W.S., Emberson, J.R., Mafham, M., Bell, J.L., Linsell, L., Staplin, N., Brightling, C., Ustianowski, A., Elmahi, E., Prudon, B., Green, C., Felton, T., Chadwick, D., Rege, K., Fegan, C., Chappell, L.C., Faust, S.N., Jaki, T., Jeffery, K., Montgomery, A., Rowan, K., Juszczak, E., Baillie, J.K., Haynes, R., Landray, M.J., 2021. Dexamethasone in hospitalized patients with covid-19. N. Engl. J. Med. 384, 693–704.

Gunther, S., Reinke, P.Y.A., Fernandez-Garcia, Y., Lieske, J., Lane, T.J., Ginn, H.M., Koua, F.H.M., Ehrt, C., Ewert, W., Oberthuer, D., Yefanov, O., Meier, S., Lorenzen, K., Krichel, B., Kopicki, J.D., Gelisio, L., Brehm, W., Dunkel, I., Seychell, B., Gieseler, H., Norton-Baker, B., Escudero-Perez, B., Domaracky, M., Saouane, S., Tolstikova, A., White, T.A., Hanle, A., Groessler, M., Fleckenstein, H., Trost, F., Galchenkova, M., Gevorkov, Y., Li, C., Awel, S., Peck, A., Barthelmess, M., Schlunzen, F., Lourdu Xavier, P., Werner, N., Andaleeb, H., Ullah, N., Falke, S., Srinivasan, V., Franca, B.A., Schwinzer, M., Brognaro, H., Rogers, C., Melo, D., Zaitseva-Doyle, J.J., Knoska, J., Pena-Murillo, G.E., Mashhour, A.R., Hennicke, V., Fischer, P., Hakanpaa, J., Meyer, J., Gribbon, P., Ellinger, B., Kuzikov, M., Wolf, M., Beccari, A.R., Bourenkov, G., von Stetten, D., Pompidor, G., Bento, I., Panneerselvam, S., Karpics, I., Schneider, T.R., Garcia-Alai, M.M., Niebling, S., Gunther, C., Schmidt, C., Schubert, R., Han, H., Boger, J., Monteiro, D.C.F., Zhang, L., Sun, X., Pletzer-Zelgert, J., Wollenhaupt, J., Feiler, C.G., Weiss, M.S., Schulz, E.C., Mehrabi, P., Karnicar, K., Usenik, A., Loboda, J., Tidow, H., Chari, A., Hilgenfeld, R., Uetrecht, C., Cox, R., Zaliani, A., Beck, T., Rarey, M., Gunther, S., Turk, D., Hinrichs, W., Chapman, H.N., Pearson, A.R., Betzel, C., Meents, A., 2021. X-ray screening identifies active site and allosteric inhibitors of SARS-CoV-2 main protease. Science 372, 642–646.

Hammond, J., Leister-Tebbe, H., Gardner, A., Abreu, P., Bao, W., Wisemandle, W., Baniecki, M., Hendrick, V.M., Damle, B., Simon-Campos, A., Pypstra, R., Rusnak, J.M., Investigators, E.-H., 2022. Oral nirmatrelvir for high-risk, nonhospitalized adults with covid-19. N. Engl. J. Med. https://doi.org/10.1056/NEJMoa2118542. Online ahead of print.

Hu, Y., Ma, C., Szeto, T., Hurst, B., Tarbet, B., Wang, J., 2021. Boceprevir, calpain inhibitors II and XII, and GC-376 have broad-spectrum antiviral activity against coronaviruses. ACS Infect. Dis. 7, 586–597.

Hung, H.C., Ke, Y.Y., Huang, S.Y., Huang, P.N., Kung, Y.A., Chang, T.Y., Yen, K.J., Peng, T.T., Chang, S.E., Huang, C.T., Tsai, Y.R., Wu, S.H., Lee, S.J., Lin, J.H., Liu, B.S., Sung, W.C., Shih, S.R., Chen, C.T., Hsu, J.T., 2020. Discovery of M Protease inhibitors encoded by SARS-CoV-2. Antimicrob. Agents Chemother. 64, e00872–20.

Iketani, S., Forouhar, F., Liu, H., Hong, S.J., Lin, F.Y., Nair, M.S., Zask, A., Huang, Y., Xing, L., Stockwell, B.R., Chavez, A., Ho, D.D., 2021. Lead compounds for the development of SARS-CoV-2 3CL protease inhibitors. Nat. Commun. 12, 2016.

Jacobs, J., Grum-Tokars, V., Zhou, Y., Turlington, M., Saldanha, S.A., Chase, P., Eggler, A., Dawson, E.S., Baez-Santos, Y.M., Tomar, S., Mielech, A.M., Baker, S.C., Lindsley, C.W., Hodder, P., Mesecar, A., Stauffer, S.R., 2013. Discovery, synthesis, and structure-based optimization of a series of N-(tert-butyl)-2-(N-arylamido)-2-(pyridin-3-yl) acetamides (ML188) as potent noncovalent small molecule inhibitors of the severe acute respiratory syndrome coronavirus (SARS-CoV) 3CL protease. J. Med. Chem. 56, 534–546.

Jain, J., Almquist, S.J., Shlyakhter, D., Harding, M.W., 2001. VX-497: a novel, selective IMPDH inhibitor and immunosuppressive agent. J. Pharmacol. Sci. 90, 625–637.

Jin, Z., Du, X., Xu, Y., Deng, Y., Liu, M., Zhao, Y., Zhang, B., Li, X., Zhang, L., Peng, C., Duan, Y., Yu, J., Wang, L., Yang, K., Liu, F., Jiang, R., Yang, X., You, T., Liu, X., Yang, X., Bai, F., Liu, H., Liu, X., Guddat, L.W., Xu, W., Xiao, G., Qin, C., Shi, Z., Jiang, H., Rao, Z., Yang, H., 2020. Structure of M(pro) from SARS-CoV-2 and discovery of its inhibitors. Nature 582, 289–293.

John Hopkins University & Medicine. Coronavirus Resource Center. https://coronavirus.jhu.edu/map.html (Accessed on 16 March 2022).

Khan, A., Ali, S.S., Khan, M.T., Saleem, S., Ali, A., Suleman, M., Babar, Z., Shafiq, A., Khan, M., Wei, D.Q., 2020. Combined drug repurposing and virtual screening strategies with molecular dynamics simulation identified potent inhibitors for SARS-CoV-2 main protease (3CLpro). J. Biomol. Struct. Dyn. 39, 4659–-4670.

Kilianski, A., Mielech, A.M., Deng, X., Baker, S.C., 2013. Assessing activity and inhibition of Middle East respiratory syndrome coronavirus papain-like and 3C-like proteases using luciferase-based biosensors. J. Virol. 87, 11955–11962.

Koes, D.R., Baumgartner, M.P., Camacho, C.J., 2013. Lessons learned in empirical scoring with smina from the CSAR 2011 benchmarking exercise. J. Chem. Inf. Model. 53, 1893–1904.

Li, S.F., Gong, M.J., Shao, J.J., Sun, Y.F., Zhang, Y.G., Chang, H.Y., 2019. Antiviral activity of merimepodib against foot and mouth disease virus in vitro and in vivo. Mol. Immunol. 114, 226–232.

Lockbaum, G.J., Reyes, A.C., Lee, J.M., Tilvawala, R., Nalivaika, E.A., Ali, A., Kurt Yilmaz, N., Thompson, P.R., Schiffer, C.A., 2021. Crystal structure of SARS-CoV-2 main protease in complex with the non-covalent inhibitor ML188. Viruses 13, 174.

Ma, C., Sacco, M.D., Hurst, B., Townsend, J.A., Hu, Y., Szeto, T., Zhang, X., Tarbet, B., Marty, M.T., Chen, Y., Wang, J., 2020. Boceprevir, GC-376, and calpain inhibitors II, XII inhibit SARS-CoV-2 viral replication by targeting the viral main protease. Cell Res. 30, 678–692.

Ma, C., Tan, H., Choza, J., Wang, Y., Wang, J., 2021. Validation and invalidation of SARS-CoV-2 main protease inhibitors using the Flip-GFP and Protease-Glo luciferase assays. Acta Pharm. Sin. B. https://doi.org/10.1016/j.apsb.2021.10.026. Online ahead of print.

Marcellin, P., Horsmans, Y., Nevens, F., Grange, J.D., Bronowicki, J.P., Vetter, D., Purdy, S., Garg, V., Bengtsson, L., McNair, L., Alam, J., 2007. Phase 2 study of the combination of merimepodib with peginterferon-alpha2b, and ribavirin in nonresponders to previous therapy for chronic hepatitis C. J. Hepatol. 47, 476–483.

Markland, W., McQuaid, T.J., Jain, J., Kwong, A.D., 2000. Broad-spectrum antiviral activity of the IMP dehydrogenase inhibitor VX-497: a comparison with ribavirin and demonstration of antiviral additivity with alpha interferon. Antimicrob. Agents Chemother. 44, 859–866.

Muramatsu, T., Takemoto, C., Kim, Y.T., Wang, H., Nishii, W., Terada, T., Shirouzu, M., Yokoyama, S., 2016. SARS-CoV 3CL protease cleaves its C-terminal autoprocessing site by novel subsite cooperativity. Proc. Natl. Acad. Sci. U. S. A. 113, 12997–13002.

O'Brien, M.P., Forleo-Neto, E., Musser, B.J., Isa, F., Chan, K.C., Sarkar, N., Bar, K.J., Barnabas, R.V., Barouch, D.H., Cohen, M.S., Hurt, C.B., Burwen, D.R., Marovich, M.A., Hou, P., Heirman, I., Davis, J.D., Turner, K.C., Ramesh, D., Mahmood, A., Hooper, A.T., Hamilton, J.D., Kim, Y., Purcell, L.A., Baum, A., Kyratsous, C.A., Krainson, J., Perez-Perez, R., Mohseni, R., Kowal, B., DiCioccio, A.T., Stahl, N., Lipsich, L., Braunstein, N., Herman, G., Yancopoulos, G.D., Weinreich, D.M., Covid-19 Phase 3 Prevention Trial Team, 2021a. Subcutaneous REGEN-COV antibody combination to prevent covid-19. N. Engl. J. Med 385, 1184–1195.

O'Brien, A., Chen, D.Y., Hackbart, M., Close, B.J., O'Brien, T.E., Saeed, M., Baker, S.C., 2021b. Detecting SARS-CoV-2 3CLpro expression and activity using a polyclonal antiserum and a luciferase-based biosensor. Virology 556, 73–78.

Owen, D., Allerton, C.M.N., Anderson, A.S., Aschenbrenner, L., Avery, M., Berritt, S., Boras, B., Cardin, R.D., Carlo, A., Coffman, K.J., Dantonio, A., Di, L., Eng, H., Ferre, R., Gajiwala, K.S., Gibson, S.A., Greasley, S.E., Hurst, B.L., Kadar, E.P., Kalgutkar, A.S., Lee, J.C., Lee, J., Liu, W., Mason, S.W., Noell, S., Novak, J.J., Obach, R.S., Ogilvie, K., Patel, N.C., Pettersson, M., Rai, D.K., Reese, M.R., Sammons, M.F., Sathish, J.G., Singh, R.S.P., Steppan, C.M., Stewart, A.E., Tuttle, J.B., Updyke, L., Verhoest, P.R., Wei, L., Yang, Q., Zhu, Y., 2021. An oral SARS-CoV-2 M(pro) inhibitor clinical candidate for the treatment of COVID-19. Science 374, 1586–1593.

Planas, D., Saunders, N., Maes, P., Guivel-Benhassine, F., Planchais, C., Buchrieser, J., Bolland, W.H., Porrot, F., Staropoli, I., Lemoine, F., Pere, H., Veyer, D., Puech, J., Rodary, J., Baele, G., Dellicour, S., Raymenants, J., Gorissen, S., Geenen, C., Vanmechelen, B., Wawina-Bokalanga, T., Marti-Carreras, J., Cuypers, L., Seve, A., Hocqueloux, L., Prazuck, T., Rey, F., Simon-Loriere, E., Bruel, T., Mouquet, H.,

Andre, E., Schwartz, O., 2021. Considerable escape of SARS-CoV-2 Omicron to antibody neutralization. Nature 602, 671–675.

Rarey, M., Kramer, B., Lengauer, T., Klebe, G., 1996. A fast flexible docking method using an incremental construction algorithm. J. Mol. Biol. 261, 470–489.

Rathnayake, A.D., Zheng, J., Kim, Y., Perera, K.D., Mackin, S., Meyerholz, D.K., Kashipathy, M.M., Battaile, K.P., Lovell, S., Perlman, S., Groutas, W.C., Chang, K.O., 2020. 3C-like protease inhibitors block coronavirus replication in vitro and improve survival in MERS-CoV-infected mice. Sci. Transl. Med. 12, eabc5332.

Rawson, J.M.O., Duchon, A., Nikolaitchik, O.A., Pathak, V.K., Hu, W.S., 2021. Development of a cell-based luciferase complementation assay for identification of SARS-CoV-2 3CL(pro) inhibitors. Viruses 13, 173.

Resnick, S.J., Iketani, S., Hong, S.J., Zask, A., Liu, H., Kim, S., Melore, S., Lin, F.Y., Nair, M.S., Huang, Y., Lee, S., Tay, N.E.S., Rovis, T., Yang, H.W., Xing, L., Stockwell, B.R., Ho, D.D., Chavez, A., 2021. Inhibitors of coronavirus 3CL proteases protect cells from protease-mediated cytotoxicity. J. Virol. 95, e0237420.

Rosas, I.O., Brau, N., Waters, M., Go, R.C., Hunter, B.D., Bhagani, S., Skiest, D., Aziz, M. S., Cooper, N., Douglas, I.S., Savic, S., Youngstein, T., Del Sorbo, L., Cubillo Gracian, A., De La Zerda, D.J., Ustianowski, A., Bao, M., Dimonaco, S., Graham, E., Matharu, B., Spotswood, H., Tsai, L., Malhotra, A., 2021. Tocilizumab in hospitalized patients with severe covid-19 pneumonia. N. Engl. J. Med. 384, 1503–1516.

Rothan, H.A., Teoh, T.C., 2021. Cell-based high-throughput screening protocol for discovering antiviral inhibitors against SARS-COV-2 main protease (3CLpro). Mol. Biotechnol. 63, 240–248.

Sacco, M.D., Ma, C., Lagarias, P., Gao, A., Townsend, J.A., Meng, X., Dube, P., Zhang, X., Hu, Y., Kitamura, N., Hurst, B., Tarbet, B., Marty, M.T., Kolocouris, A., Xiang, Y., Chen, Y., Wang, J., 2020. Structure and inhibition of the SARS-CoV-2 main protease reveal strategy for developing dual inhibitors against M(pro) and cathepsin L. Sci. Adv. 6, eabe0751.

Shionogi. Top-Line Results of the Phase 2a Part of the Phase 2/3 Trial of S-217622. https ://www.shionogi.com/global/en/investors/ir-library/presentation-materials.html. (Accessed on 16 March 2022).

Su, H.X., Yao, S., Zhao, W.F., Li, M.J., Liu, J., Shang, W.J., Xie, H., Ke, C.Q., Hu, H.C., Gao, M.N., Yu, K.Q., Liu, H., Shen, J.S., Tang, W., Zhang, L.K., Xiao, G.F., Ni, L., Wang, D.W., Zuo, J.P., Jiang, H.L., Bai, F., Wu, Y., Ye, Y., Xu, Y.C., 2020. Anti-SARS-CoV-2 activities in vitro of Shuanghuanglian preparations and bioactive ingredients. Acta Pharmacol. Sin. 41, 1167–1177.

Tong, X., Smith, J., Bukreyeva, N., Koma, T., Manning, J.T., Kalkeri, R., Kwong, A.D., Paessler, S., 2018. Merimepodib, an IMPDH inhibitor, suppresses replication of Zika virus and other emerging viral pathogens. Antivir. Res. 149, 34–40.

Tummino, T.A., Rezelj, V.V., Fischer, B., Fischer, A., O'Meara, M.J., Monel, B., Vallet, T., White, K.M., Zhang, Z., Alon, A., Schadt, H., O'Donnell, H.R., Lyu, J., Rosales, R.,

McGovern, B.L., Rathnasinghe, R., Jangra, S., Schotsaert, M., Galarneau, J.R., Krogan, N.J., Urban, L., Shokat, K.M., Kruse, A.C., Garcia-Sastre, A., Schwartz, O., Moretti, F., Vignuzzi, M., Pognan, F., Shoichet, B.K., 2021. Drug-induced phospholipidosis confounds drug repurposing for SARS-CoV-2. Science 373, 541–547.

Turlington, M., Chun, A., Tomar, S., Eggler, A., Grum-Tokars, V., Jacobs, J., Daniels, J.S., Dawson, E., Saldanha, A., Chase, P., Baez-Santos, Y.M., Lindsley, C.W., Hodder, P., Mesecar, A.D., Stauffer, S.R., 2013. Discovery of N-(benzo[1,2,3]triazol-1-yl)-N-(benzyl)acetamido)phenyl carboxamides as severe acute respiratory syndrome coronavirus (SARS-CoV) 3CLpro inhibitors: identification of ML300 and noncovalent nanomolar inhibitors with an induced-fit binding. Bioorg. Med. Chem. Lett 23, 6172–6177.

Ullrich, S., Nitsche, C., 2020. The SARS-CoV-2 main protease as drug target. Bioorg. Med. Chem. Lett 30, 127377.

US Food and Drug Administration. Coronavirus (COVID-19) Drugs. https://www.fda.gov /drugs/emergency-preparedness-drugs-coronavirus-covid-19-drugs. (Accessed on 16 March 2022).

V'Kovski, P., Kratzel, A., Steiner, S., Stalder, H., Thiel, V., 2021. Coronavirus biology and replication: implications for SARS-CoV-2. Nat. Rev. Microbiol. 19, 155–170.

ViralClear Press release. ViralClear halts its Phase 2 Hospitalized COVID-19 Trial. doi: https://ir.biosig.com/press-releases/detail/234/viralclear-halts-its-phase-2-hospital ized-covid-19-trial (Accessed 16 March 2022).

Vuong, W., Khan, M.B., Fischer, C., Arutyunova, E., Lamer, T., Shields, J., Saffran, H.A., McKay, R.T., van Belkum, M.J., Joyce, M.A., Young, H.S., Tyrrell, D.L., Vederas, J.C., Lemieux, M.J., 2020. Feline coronavirus drug inhibits the main protease of SARS-CoV-2 and blocks virus replication. Nat. Commun. 11, 4282.

Wang, Q., Zhao, Y., Chen, X., Hong, A., 2020. Virtual screening of approved clinic drugs with main protease (3CL(pro)) reveals potential inhibitory effects on SARS-CoV-2. J. Biomol. Struct. Dyn. 40, 685–695.

Zhang, L., Lin, D., Sun, X., Curth, U., Drosten, C., Sauerhering, L., Becker, S., Rox, K., Hilgenfeld, R., 2020. Crystal structure of SARS-CoV-2 main protease provides a basis for design of improved alpha-ketoamide inhibitors. Science 368, 409–412.

Zhao, Y., Fang, C., Zhang, Q., Zhang, R., Zhao, X., Duan, Y., Wang, H., Zhu, Y., Feng, L., Zhao, J., Shao, M., Yang, X., Zhang, L., Peng, C., Yang, K., Ma, D., Rao, Z., Yang, H., 2021. Crystal structure of SARS-CoV-2 main protease in complex with protease inhibitor PF-07321332. Protein Cell. https://doi.org/10.1007/s13238-021-00883-2.

Zhu, W., Xu, M., Chen, C.Z., Guo, H., Shen, M., Hu, X., Shinn, P., Klumpp-Thomas, C., Michael, S.G., Zheng, W., 2020. Identification of SARS-CoV-2 3CL protease inhibitors by a quantitative high-throughput screening. ACS Pharmacol. Transl. Sci. 3, 1008–1016.